Bräuer, K., Kämpf, H., Niedermann, S., **Strauch, G.** (2018):
Monitoring of helium and carbon isotopes in the western Eger Rift area (Czech Republic): Relationships with the 2014 seismic activity and indications for recent (2000–2016) magmatic unrest
Chem. Geol. **482** , 131 – 145

http://dx.doi.org/10.1016/j.chemgeo.2018.02.017

Monitoring of helium and carbon isotopes in the western Eger Rift area (Czech Republic): Relationships with the 2014 seismic activity and indications for recent (2000 – 2016) magmatic unrest

Karin Bräuer[a*], Horst Kämpf[b], Samuel Niedermann[b], Gerhard Strauch[a]

[a]UFZ-Helmholtz Centre for Environmental Research, Germany

[b] GFZ German Research Centre for Geosciences, Germany

* Corresponding author

Abstract

We report new data of the regional distribution pattern of total gas compositions as well as He and CO_2 isotopic compositions from 25 gas exhalations in the western Eger Rift and its surroundings. Additionally, the first time-series data from gas exhalations in a clay pit within the Cheb Basin (CB) are given. At 21 degassing locations, the first data were obtained more than 20 years ago. From 7 locations within the degassing center CB and from 3 degassing sites belonging to the Mariánské Lázně (ML) degassing center, neon and argon isotope compositions were determined also.

CO_2 is the major component at all degassing sites. The $\delta^{13}C$ values display a small range (-1.7 to -5.1‰) and the $^3He/^4He$ ratios vary from 1.9 to 5.9 R_a. The highest $^3He/^4He$ ratios are found at locations along the Počatky-Plesná Fault Zone, followed by the degassing site in the clay pit on the Nová Ves Fault and the locations on the ML fault at the edge of the CB. Although gas flow and CO_2 concentrations in all degassing centers are very high, the fractions of mantle-derived helium are different, with presently up to 94% (in relation to the SCLM $^3He/^4He$ of 6.32 R_a) in the CB, up to 73% in the ML and up to 35% in the Karlovy Vary degassing center. At the locations in the eastern part of the CB a clear, progressive increase of the $^3He/^4He$ ratio has been observed since the first sampling campaigns there in 1993 and

1994, whereas at the other degassing sites the helium isotope ratio remained essentially the same. The progressive increase of the $^3He/^4He$ ratio in the eastern part of the CB, together with further short-time increases up to 6.3 R_a at one location (Bublák) before both the 2000 and 2008 earthquake swarms, indicate an ongoing magmatic process beneath this area, which seems to be associated with the occurrence of seismicity. The CB is located close to the Nový Kostel focal zone where since the beginning of our investigations four strong periods of seismicity (with magnitudes >3) occurred. The latest gas data confirm our earlier findings: time-series studies showed that in relation with seismic events, decreased $^3He/^4He$ ratios were repeatedly observed due to admixed seismically released crustal helium. Presently, the eastern part of the CB is the most active non-volcanic region in the European Cenozoic Rift System, with gas signatures similar to those found in free mantle-derived gases from the East African Rift system.

Keywords:

Eger Rift; SCLM; Magmatic CO_2; Noble Gases; $^3He/^4He$ ratios; $\delta^{13}C_{CO2}$

Highlights

- First time-series data of gas compositions and He and C isotope ratios from a degassing site in a clay pit are given.
- N_2, Ar and Ne isotope ratios indicate mixing between mantle and air-derived components along the Počatky-Plesná Fault Zone.
- The SCLM signature of Cheb Basin gas is similar to that reported for free gas of the East African Rift.
- The eastern part of the Cheb Basin is presently the most active area within the European Cenozoic Rift system.

1. Introduction

The investigation area in the western Eger Rift (NW Bohemia; Fig. 1) is part of the European Cenozoic Rift System (ECRIS) (Ziegler, 1992) and is known for the recurrence of earthquake swarms (e.g. Fischer et al., 2014 and references therein). This type of seismicity is mainly known from volcanically active areas (e.g. Hill, 1977; Sigmundsson et al., 1997; Schlindwein, 2012) but also occurs in non-volcanic areas, associated with deep-reaching zones of weakness in continental rifts (Ibs-von Seht et al., 2008). In addition, the region is characterized by the presence of CO_2-rich springs and mofettes (e.g. Pačes, 1974; 1987), which are used for medical treatment in the well-known spas of Františkovy Lázně, Mariánské Lázně, and Karlovy Vary.

Such CO_2-rich degassing sites are also known from other rift (graben) structures within the ECRIS, and most of them are associated with Quaternary volcanism such as in the Eifel area, Germany (e.g. Griesshaber et al., 1992; Bräuer et al., 2013) or in the French Massif Central (e.g. Matthews et al., 1987; Aeschbach-Hertig et al., 1996; Battani et al., 2010; Bräuer et al., 2017). Likewise, seismicity occurs also in the Eifel area (e.g. Hinzen, 2003) as well as in the Massif Central (e.g. Mazabraud et al., 2005), but not as intense as in NW Bohemia.

Between 1992 and 1994, Weinlich et al. (1999) studied 74 degassing sites in the western Eger Rift area in detail by measuring the gas composition, the gas flow and the isotope ratios of CO_2 and helium. As a result, the regional distribution patterns revealed three discrete degassing centers: the Cheb Basin (CB), Mariánské Lázně and surroundings (ML), and Karlovy Vary (KV). They are all characterized by high gas flow, nearly pure CO_2 and high fractions of mantle-derived helium, therefore indicating a predominantly mantle-derived origin of both CO_2 and helium.

Geochemical fluid investigations in seismically active areas worldwide have reported anomalies of gas and isotopic compositions due to seismic unrest, pointing to seismically induced mobilization of fluids in the earth's crust and changes of fluid transport and of the permeability of migration paths (e.g. Sugisaki and Sugiura, 1986; Hilton, 1996; Sano et al., 1998; Toutain and Baubron, 1999; Caracausi et al., 2005; Chiodini et al., 2011). Seismically triggered anomalies due to several strong earthquake swarms were also recorded in NW Bohemia in the course of detailed monitoring studies of the gas and isotopic compositions (e.g. Bräuer et al., 2003; 2008; 2011). Otherwise, time-series studies to trace geochemical variations of degassing fluids or geochemical long-term studies have mainly been carried out at active volcanos (e.g. Lee et al., 2008; Martelli et al., 2008; Werner et al., 2009; Chiodini et al., 2010; Vaselli et al., 2010).

The goal of our new investigations was to reevaluate the geodynamic situation in the Eger Rift area after the occurrence of four seismically active periods (2000, 2008, 2011, and 2014) in the Nový Kostel (NK) epicentral area (Fischer et al., 2014; Hainzl et al., 2016). We present new data of the gas and isotopic compositions recorded during several sampling campaigns between 2014 and 2016 and additional monitoring data (March 2001 to August 2014) of a degassing site in a clay pit near Skalná, where monthly samples were taken from April 2010 to December 2011. As a result, we establish and/or concretize the role of the regional degassing structures.

2. Geological background

The investigation area is located within the transition zone of the Saxothuringian, the Teplá-Barrandian and the Moldanubian – a triple junction of three separated Variscan structural units (Babuška et al., 2007). In the Early Triassic, the units were reactivated, and they have presumably remained active to the present day. The evolution of the Eger Rift, which is part of the European Cenozoic Rift System (ECRIS; Ziegler, 1992), was probably associated with the occurrence of magmatic activity during the Cenozoic. Four volcanoes with Quaternary volcanic activity are known in this area (Fig. 1). The two scoria cones Železná hůrka (ZH) and Komorní hůrka (KH) are well-known. In addition, two maar structures have recently been identified: the Mýtina maar (MM; Mrlina et al., 2009) and the Neualbenreuth Maar (NM; Rohrmüller et al., 2017). All these volcanic features are located on the Tachov Fault (TF; Fig.1).

Many seismological studies were carried out in order to search for structural discontinuities within the lithosphere beneath the investigation area. Using receiver functions, Geissler et al. (2005) and Heuer et al. (2006) found indications for crustal thinning from about 31 km to 27 km. The results of Heuer et al. (2011), who evaluated the structure of the lithosphere beneath western Bohemia, confirmed the Moho updoming there and additionally pointed to the existence of a plume-like structure beneath western Bohemia, but with only little or no imprint on the 410 km discontinuity. Further detailed active and passive seismic investigations found hints for a gradational zone over about 5 km, rather than a sharp discontinuity at the crust/mantle boundary (Hrubcová and Geissler, 2009). This interpretation of a laminated Moho structure, with a transition zone that varies between 2 and 4 km in thickness at depths ranging from 27 km to 31.5 km, was supported by Hrubcová et al. (2013).

The repeated occurrence of intraplate earthquake swarms demonstrates the recent geodynamic activity of the region. Since the strong earthquake swarm in 1985/1986 (Grünthal et al., 1990), another four strong earthquake swarms occurred in 2000 (Fischer and Horálek, 2003), 2008 (Fischer et al., 2010), 2011 (Fischer et al., 2014) and 2014 (Hainzl et al., 2016). All were focused on the Nový Kostel focal zone (Fig. 1). The latest seismically active period in 2014 overlapped spatially with previous swarm activity, but consisted of three classical aftershock sequences triggered by magnitude 3.5, 4.4, and 3.5 events. Hainzl et al. (2016) have proposed a system change of the seismicity from swarm-type to mainshock-aftershock characteristics.

3. Locations and techniques

The sampling locations (Fig. 1) were selected based on earlier results of the regional distribution pattern of gas and isotope signatures from more than 100 degassing sites in NW Bohemia sampled between 1992 and 2001 (Weinlich et al., 1999; Geissler et al., 2005). Our investigations focus on gas-rich locations within the three degassing centers as well as on some at their peripheries (Fig. 1). Part of these degassing sites had been repeatedly studied during the last 20 years (e.g. Bräuer et al., 2005b, 2008, 2009). The geological background of the sampling location in the clay pit Nová Ves II, near Skalná (no.91), was described by Bankwitz et al. (2003). These authors detected an ENE striking shear zone within the clay pit, whereas usually the Cheb Basin is characterized by N-S trending faults.

Gas sampling was always carried out in the same way. We used glass vessels made of AR glass, which belongs to the soda lime group and contains a high portion of alkali and alkaline earth oxides. This type of glass is known to have a very low permeability for helium. Samples from the free gas phase were taken after passage through surficial water bodies. The evacuated vessels were first filled with spring water, and subsequently gas bubbles were collected by means of a funnel, thereby replacing the water in the vessel. Duplicate samples were always taken; one was used for measuring the total gas composition and the second one was split for the measurements of the isotope ratios of helium and CO_2, and partly also the isotope ratios of nitrogen, neon and argon. For analyzing the gas composition, 2 L glass vessels were commonly used because in general the non-acid fraction of the gas was very small. Therefore, in the lab, CO_2 was absorbed in KOH solution (17.8 mol/L) and the CO_2 content was determined volumetrically, taking into account the volume of the non-acid gas and the volume of the glass vessel. The precision of the volumetrical CO_2 determinations is ± 0.1 mL. The non-acid gas fraction, such as N_2, O_2, Ar, He, H_2, and CH_4, was analyzed by gas chromatography with higher accuracy after removing CO_2 by absorption in KOH solution (Weinlich et al., 1998). Columns, carriers and detectors were selected in relation to the components to be determined. The precision of the gas chromatographic determination of N_2 and O_2 contents is ± 3% (relative) and that of the minor components Ar, He, H_2, and CH_4 is ± 10-40% (relative).

For $\delta^{13}C$ analyses, CO_2 and water were separated from the non-condensable gases by a two-step cryogenic separation in vacuum at liquid nitrogen temperature. Water vapor was removed by a mixture of dry ice and alcohol at –78°C. The isotope analysis of carbon was carried out using a Finnigan MAT Delta-S mass spectrometer. The standard deviation of the $\delta^{13}C$ measurement is <0.05 ‰. The $\delta^{13}C$ values were related to PDB and the reproducibility of the $\delta^{13}C$ was < 0.1‰.

The isotope analyses of nitrogen and the noble gases were carried out on the small fraction of non-condensable residual gas remaining after the two-step cryogenic separation. The gas was split into two small AR-glass tubes, one of which was used for the measurement of the N isotope composition and the second one for noble gas isotope analyses (see below). The $\delta^{15}N$ values are related to an air nitrogen standard, the standard deviation of the $\delta^{15}N$ measurement is < 0.1 ‰ and the reproducibility of the $\delta^{15}N$ value is ±0.2 ‰. After each isotope measurement a mass scan was carried out, in which the intensities of the mass 32 and 40 peaks were monitored in order to check for a possible atmospheric contamination introduced by sample handling. The comparison of the oxygen and argon concentrations from the determination of the gas composition (performed in a separate sample) and from the isotope measurement would reveal such a contamination.

In order to determine the $^{3}He/^{4}He$ ratios, the second AR glass ampoule was connected to a fully automated noble gas mass spectrometer system equipped with a two-stage cryo-system. Helium and neon were separated from other gases in the first cryo-trap by cooling a stainless steel tube to 25 K. A split was then analyzed for $^{4}He/^{20}Ne$ using a sensitive quadrupole mass spectrometer. The remaining He and Ne were transferred to a second cryo-trap at a temperature of 14 K, where the gases were adsorbed onto activated charcoal. Through precise temperature control the helium was then desorbed at 45K and transferred to a dedicated sector field mass spectrometer (MAP 215-50®), in which ^{3}He was separated from HD molecules; the ^{3}He was then detected using a Channeltron electron multiplier and ^{4}He using a Faraday cup (Sültenfuß et al., 2009). The precision of the helium isotope measurement is < 2%.

For ten degassing locations (Table 2), also neon and argon isotopes were analyzed in addition to helium in a VG5400 mass spectrometer at GFZ Potsdam. Depending on noble gas partial pressures in the AR glass tubes, appropriate volume splits were admitted to the purification line and sequentially exposed to a dry ice-cooled cold trap, two Ti sponge getters and two SAES (Zr-Al) getters. Ar, Kr and Xe were adsorbed to a stainless steel frit at 50 K and He and Ne to activated charcoal at 11 K. Mass spectrometric analysis was performed individually for He, Ne, and Ar after release from the cold traps at 35 K, 120 K, and 150 K, respectively. More details about analytical procedures and data evaluation methods can be found in Niedermann et al. (1997); the precision of the results is reported in Table 2.

4. Results

The geographic locations of the sampling sites are shown in Fig. 1. The location numbers are the same as used in the earlier studies of the free gas phase (Weinlich et al., 1999; Geissler et al., 2005). For our evaluation of the long-term trends of the fluid signatures within the distinguished degassing centers, locations with high gas flow were selected.

4.1 Regional long-term distribution pattern

At 21 sampling sites, the free gas phase was characterized in detail (field data, gas composition and isotope ratios of CO_2, He, partly Ne and Ar) for the first time after 20 years. Additionally, the Wettinquelle in Bad Brambach (no. 14a) and a degassing site in a clay pit near Skalná (Nová Ves II, no. 91) were studied in detail again since 2000 and 2001, respectively. Besides that, we also present free gas data obtained from two boreholes (nos. 111 and 112) in the Hartoušov mofette field (Kämpf et al., 2013) close to the Hartoušov mofette (no. 24, Fig. 1). The complete data are given in Tables 1, 2, and 3.

4.1.1 Gas composition

The major gas component at all studied degassing locations is CO_2. With the exception of Kopanina (no. 21) and Křepkovice (no. 61) - two locations with low gas flow – the CO_2 concentration was always clearly higher than 90 vol. %. At the latter locations (nos. 21 and 61) the gas/water ratio is < 0.02 (Weinlich et al., 1999). The relative abundances of the non-reactive components N_2, He and Ar are shown in two ternary diagrams (Fig. 2a,b). Most data plot in the field bounded by the mixing lines between mantle-derived origin, air-saturated water (ASW), and air.

4.1.2 $\delta^{13}C$ and $^3He/^4He$

Overall, the measured $\delta^{13}C$ values are negative. The range of $\delta^{13}C$ values is small. Altogether, they vary between -5.1‰ and -1.7‰ (Table 1) and, for locations within the degassing centers (characterized by high gas flow; Fig. 1), only between -3.6‰ and -1.9‰ (Fig. 3). The

$CO_2/^3He$ ratios vary over three orders of magnitude from 2.7×10^8 to 9.6×10^{11}, but are $<10^{10}$ at all mofettes, apart from the mofette Soos (no. 26).

The reported $^3He/^4He$ ratios have been air-corrected using the He/Ne ratios and are given in R_a units, i.e. the measured air-corrected $^3He/^4He$ ratios were divided by the $^3He/^4He$ of air ($^3He/^4He_{air}=1.384 \times 10^{-6}$). The $^3He/^4He$ ratios vary between 1.9 R_a and 5.9 R_a. The range within the degassing centers (Fig. 1) is smaller. However, maximum contributions of mantle-derived helium are different in the three degassing centers. In the CB, the $^3He/^4He$ ratios range between 3.6 R_a and 5.9 R_a, in the ML degassing center they are between 3.2 R_a and 4.6 R_a, and the only location sampled in the KV degassing center (no. 94) indicates a low fraction of mantle-derived helium (2.2 R_a).

4.1.3 Neon and argon isotope ratios

At 10 degassing locations also the neon and argon isotope compositions were determined (Table 2). The neon isotope ratios are close to the atmospheric values (Fig. 4). The $^{20}Ne/^{22}Ne$ ratios (air: 9.80) range up to 10.26 and the $^{21}Ne/^{22}Ne$ ratios (air: 0.0290) to 0.0326. To evaluate the deviations of the Ne isotopic compositions from air, we used the $\delta^{20}Ne$ and $\delta^{21}Ne$ notation, with $\delta^xNe=[(^xNe/^{22}Ne_{sample})/(^xNe/^{22}Ne_{air})-1] \times 100$ and $^xNe=^{20}Ne$ or ^{21}Ne. The δ^{20} and δ^{21} values are given in Table 2 also.

If $^{20}Ne/^{22}Ne$ and $^{21}Ne/^{22}Ne$ ratios above the atmospheric values are solely due to isotopic mass fractionation, we expect $\delta^{20}Ne \approx 2\times\delta^{21}Ne$. This effect is obvious at the Mariiny mofette (no. 46). That degassing site is used for CO_2 treatments in the Mariánské Lázně spa and was reconstructed after 2006. Figure 4 includes neon isotope data of the Mariiny mofette gas before and after the reconstruction, showing values close to air before reconstruction and a strong mass fractionation effect thereafter. To a smaller extent, mass fractionation seems to have occurred also at the Soos mofette (no. 26). Conversely, $\delta^{20}Ne<\delta^{21}Ne$ ratios were found at the mofettes Bublák (no. 23), Smrad'och (43) and possibly at Hartoušov (24), and most clearly in the two boreholes (nos. 111 and 112) in the Hartoušov mofette field (Fig. 4).

The $^{40}Ar/^{36}Ar$ ratios span a large range, from ratios close to atmospheric (298.56) up to $^{40}Ar/^{36}Ar$ ≈1430. The lowest $^{40}Ar/^{36}Ar$ ratio of 291.4 is lower than the atmospheric ratio and was measured in the Mariiny mofette gas (no. 46) after its reconstruction. It is probably due to mass fractionation, as already discussed for the neon isotope ratios (Fig. 4) and further supported by the low $^{38}Ar/^{36}Ar$ ratio of 0.1844 (air: 0.1885). The highest $^{40}Ar/^{36}Ar$ ratios were measured in the gas from the two boreholes in the Hartoušov mofette field, where also the highest $^{21}Ne/^{22}Ne$ ratios were found (Table 2).

4.2 Time-series gas data recorded in the clay pit Nová Ves II near Skalná

All data from the degassing site in the clay pit are given in Table 3. We started to study this site in 2001, taking samples at four different places in the clay pit. There was little evidence for a significant difference in the gas characteristics between these degassing locations. The mean CO_2 concentration was 99.7 ± 0.2 vol.% and the $\delta^{13}C$ value -2.2 ± 0.1‰ (Bankwitz et al., 2003). It was difficult to take samples from the same location during progressive mining of the clay. Therefore, between 2003 and 2008 samples were taken at different places close to the 2001 locations. Since April 2010, we took samples for a monthly time-series from the same location (Fig. 5). The time series data (Fig. 6) depict variations of the CO_2 (99.5±0.3 vol.%) and helium contents (23±4 ppmv), but these do not correlate with water temperature. The $^{3}He/^{4}He$ ratios range between 5.3 and 5.7 R_a and the $\delta^{13}C$ values between -2.4 and -2.1‰. The $CO_2/^{3}He$ ratios vary between 3.8×10^{9} and 6.5×10^{9} and the $\delta^{15}N$ values between -2.5 and +1.2‰.

5. Discussion

The first spatially extensive investigation of the free gas phase at degassing sites in NW Bohemia (74 sites) was carried out between 1992 and 1994 (Weinlich et al., 1999) and was later expanded to a larger area and to 101 degassing sites (Geissler et al., 2005). The first study characterized the gas signatures with respect to the origin of the gases and their modification during migration from the degassing source to the surface (Weinlich et al., 1999). Subsequently, several time-series studies were carried out (e.g. Bräuer et al., 2004, 2005a, 2008, 2011, 2014), aiming at obtaining more detailed information about the processes affecting the gas signatures with respect to the prevailing geodynamic situation. The western Eger Rift area is unique in Europe because of the recurrence of earthquake swarms in a non-volcanic area and for showing indications of presently ongoing hidden magmatic processes in the subcontinental lithospheric mantle (Bräuer et al., 2005b, 2009). At Long Valley caldera (California), where the last eruptions occurred about 600 years ago (e.g. Eichelberger et al., 1988), the first isotope-geochemical time series studies at fumaroles and springs proved to be a useful tool to monitor seismically and magma-driven changes of the fluid signatures (Hilton, 1996). The temporal and spatial frames of such a complex magma/fluid-driven process were assessed by Hill and Prejean (2005) based on combined geochemical and seismological long-term studies from Long Valley caldera.

The project presented here was focused on the evolution of gas signatures in the Eger Rift area after the occurrence of three earthquake swarms (2000, 2008 and 2011). The 2000 and 2008 swarms had been accompanied by detailed monitoring of the gas and isotopic compositions (e.g. Bräuer et al., 2008, 2014). Based on these studies we knew that within a period of two years after the beginning of the seismically active period an admixture of crustal components could occur repeatedly. The aim of the new project was to repeat the characterization of gas signatures in a period of seismic quiescence to avoid seismically triggered modifications. However, at almost the same time with our first field trip in 2014 a further earthquake series started in late May of that year. For this reason we repeated the sampling in the CB in 2015 and 2016 (Table 1). In the correlations described below, the data from the 2016 sampling were used, which should be free of seismically triggered variations. In contrast to the CB, no impact of seismicity occurring in the NK focal zone on the gas signatures in the ML and KV degassing centers has been observed to date.

5.1. Revisiting the characteristics of gas exhalations in the western Eger Rift area

The $\delta^{13}C$ values of the selected degassing locations (Table 1) are nearly equal to those recorded 20 years ago (Weinlich et al., 1999). Deviations of clearly more than 0.1 ‰ were only found in mineral springs with extremely low gas/water ratios (nos. 21, 61, 73) and at a pumped spring (no. 41). Time-series data of gas compositions and $\delta^{13}C$ values at mineral springs reveal seasonal variations, however. E.g., Bräuer et al. (2008) discussed in detail chemical and isotopic fractionation processes which can modify the gas and isotopic signatures. In general, the CO_2 at degassing locations within the CB is more enriched in ^{13}C than MORB. Detailed studies of the Bublák mofette gas (e.g. Bräuer et al., 2004) implied that its $\delta^{13}C$ signature is mostly derived from the supplying magmatic reservoir. The reason for $\delta^{13}C$ values greater than MORB may be smaller gas/melt ratios in the SCLM than in MORB (Ballentine, 1997) and/or effects of the different composition and degassing state of the supplying magmatic reservoir (Dunai and Porcelli, 2002). Fischer et al. (2009) found similar ^{13}C-enriched carbon in the East African Rift (EAR) in the gas phase of the erupting Oldoinyo Lengai volcano. They supposed that the gas stems from the silicate portion of the magmatic system that originates in the upper mantle. The sample with the highest $^{40}Ar/^{36}Ar$ ratio (948) was characterized by a $\delta^{13}C$ value of -2.4 ‰ and a $CO_2/^3He$ ratio of 4.13 x10^9; the $^3He/^4He$ ratios in the gas from the erupting Oldoinyo Lengai were ~6.7 Ra, which is somewhat higher than in the Bublák gas. The EAR is the most prominent continental rift system. Seismic studies indicate a 670 km seismic discontinuity, pointing to a plume structure beneath that region. Similarly, in the upper mantle below the western Bohemia earthquake region Heuer et al. (2011) found indications for a plume-like structure in receiver function studies, but with no or only a weak imprint on the 410 km discontinuity.

Investigations of the $^3He/^4He$ ratios of volcanic rocks from the Rungwe Volcanic Province (RVP), belonging also to the EAR, found plume-like $^3He/^4He$ ratios up to 15 R_a pointing to magma contributions originating deeper than the continental lithospheric mantle there (Hilton et al., 2011). Free fluids in the RVP show a wide range of $^3He/^4He$ ratios, $\delta^{13}C$ values and $CO_2/^3He$ ratios. However, at some cold CO_2 gas vents the upper mantle signature does not seem to be modified by the hydrothermal system (Barry et al., 2013; de Mohr et al., 2013). Barry et al. (2013) assume that gas from previous eruptions was trapped and isolated from the hydrothermal system and in this way retained the upper mantle signature. The gas characteristic ($^3He/^4He$, $\delta^{13}C$, $CO_2/^3He$) of the cold gas vents is comparable to that of gas vents in the ECRIS. As a representative of the European subcontinental mantle signature, we use the Escarot degassing site, which is located close to the youngest volcano in the ECRIS, Lac Pavin (French Massif Central) (Bräuer et al., 2017) and has a gas signature ($^3He/^4He \approx 6.2$ R_a, $\delta^{13}C \approx -3.7$‰, $CO_2/^3He \approx 4.2 \times 10^9$) characterized by the highest $^3He/^4He$ ratios of gas vents in the ECRIS.

Figure 7 shows $^3He/^4He$ (uncorrected for air contamination) versus He/Ne ratios and illustrates the predominantly mantle-derived origin of the gas. The gas from mofettes along the PPZ plots within the SCLM range. As most He/Ne ratios are rather high, the contribution of atmospheric helium is negligible, but small contributions of crustal helium are indicated at most degassing locations. Figures 8, 9 and 10 support this statement. For more clarity, the data from the CB and surroundings and those from ML and surroundings are shown in two separate panels of Fig. 8 (a and b, respectively). In the CB, the $^{3}He/^{4}He$ ratios of the mofettes and of the two boreholes are within the SCLM range while the ML $^{3}He/^{4}He$ ratios are dominated by mantle-derived gas also, but do not quite reach the SCLM level.

In the CB and ML degassing centers, there are gas vents with higher $CO_2/^{3}He$ ratios and clearly lower helium concentrations than postulated for mantle-derived origin (Javoy and Pineau, 1991), while others have lower $CO_2/^{3}He$ ratios and higher helium concentrations than assumed for SCLM (Fig. 9a). Only few $CO_2/^{3}He$ data are available for mantle-derived xenoliths from the SCLM, ranging from the MORB value ($2x10^{9}$) up to 10^{13} (Dunai and Porcelli, 2002). Therefore, we use the data from the Escarot degassing site (French Massif Central; $CO_2/^{3}He$= 4.13 $x10^{9}$) as reference for the SCLM (Bräuer et al., 2017). Figure 9b shows $CO_2/^{3}He$ vs. $\delta^{13}C$ values and depicts also effects due to occurring chemical fractionation supplemented by effects of isotope fractionation due to different gas/water ratios. All $\delta^{13}C$ values cover a narrow range. Isotope fractionation due to different gas/water ratios can be neglected for the mofettes, whose $\delta^{13}C$ values range from -3 to -2‰, whereas the free gas phase of mineral springs has mostly smaller $\delta^{13}C$ values (< -3.5‰). Isotope fractionation depends on gas/water ratios, water temperature and mineralization (e.g. Bräuer et al., 2008). Low mineralized springs with small gas/water ratios (nos. 21 and 61) are an exception. Here the isotope fractionation is dominated by the formation of dissolved CO_2 and results in ^{13}C enrichment in the gas of the two springs (Fig. 9b, Table 1). Both figures (9a and b) reflect the influence of chemical fractionation, again most clearly visible for the locations Kopanina (no. 21) and Křepkovice (no. 61) with extremely low gas/water ratios (Weinlich et al., 1999). Due to the much higher solubility of CO_2 in water compared with the non-acid gas components, a depletion of CO_2 and thus a relative enrichment of the non-acid gas components takes place in the gas phase (e.g. Zartman et al., 1961; Ballentine et al., 1991; Bräuer et al., 2008). Indeed, the highest helium concentrations together with the lowest $CO_2/^3He$ ratios were recorded in the gas from these locations (Fig. 9a).

Figure 8 shows that a wide range of $CO_2/^3He$ ratios is observed at the different degassing sites despite little variation in $^3He/^4He$. Therefore, the spread in the $CO_2/^3He$ ratios cannot be explained by a simple mixing process between a mantle and a crustal endmember alone. Locations with $CO_2/^3He$ ratios $>10^{10}$ are characterized by helium concentrations clearly lower than in the gas from the Escarot site (Fig. 9a) and from the mofettes along the PPZ. The inverse correlation between $CO_2/^3He$ ratios and helium concentrations in the gases (Fig. 9a) indicates a preferential loss of helium by stripping during migration (e.g. van Soest et al., 1998; Snyder et al., 2001; de Leeuw et al., 2010). In contrast, locations with helium concentrations higher than found in the gas phase of popping rocks (about 33 ppmv; Javoy and Pineau, 1991) may indicate, in addition to chemical fractionation effects, an admixture of crustal helium, which is supported by lower $^3He/^4He$ ratios (Table 1). Nevertheless, at the locations 26, 27, 29, 42, 52, and 56 the reason for $CO_2/^3He >10^{10}$ (Figs. 8 and 9) seems to be the migration of mantle-derived fluids away from deep-reaching conduits at shallow level that results in a preferential loss of helium by stripping near the surface.

The ternary ^4He-CO_2-^3He plot (Fig. 10) may help to identify possible processes (arrows) which have dominantly influenced the gas signatures, such as binary mixing of gases and loss or addition of a particular gas component. The data close to the CO_2 apex gives evidence for the occurrence of helium loss at some degassing sites of the CB and ML degassing centers. Their relatively high $^3He/^4He$ ratios demonstrate that the fractionation process must have taken place at the end of the gas migration near the surface without changing the He isotope ratios. As already mentioned above, the degassing sites nos. 21 and 61 have the lowest gas/water ratios (Weinlich et al., 1999) and thus are most strongly influenced by chemical fractionation, i.e. CO_2 loss and enrichment of the non-acid components in the gas phase. These two degassing sites are located at the boundaries of the respective degassing centers, so in addition to chemical fractionation also the admixture of crustal helium during migration away from the deep reaching degassing channel may be significant. The data from the mofette fields along the PPZ (Fig. 10a) are closest to the SCLM signature, whereas the mofette data from the ML degassing center show an admixture of radiogenic helium (Fig. 10b). Although gas flow and CO_2 concentration in all degassing centers are very high, the contribution of mantle-derived helium is different. Bräuer et al. (2008) proposed that the degassing centers could be supplied by separated magmatic reservoirs at the crust/mantle boundary. Based on seismic data from reflection and refraction profiles and from local seismicity, Hrubcová et al. (2017) identified significant lateral variations of the high velocity lower crust and combined the new findings with results of fluid and petrological studies. They showed that the distribution of mantle-derived degassing at the surface correlates with the position and extent of the magma body in the lower crust. The high $^3He/^4He$ ratios of the mofettes in the CB evince a recent magmatic origin. In summary, active magmatic underplating is indicated in the western Eger Rift.

It is commonly accepted that helium is a reliable tracer to determine the origin of fluids from different reservoirs. Although neon and argon isotope ratios are much more affected by addition of atmospheric components due to their higher abundances in the atmosphere, they are nevertheless useful to identify or confirm processes which have influenced the gas signatures. From 7 locations in the CB and 3 in the ML degassing center, Ne and Ar isotope ratios were measured along with He (Table 2). With the exception of Prameny (no. 38), all other sites show mofette-type degassing. Along the PPZ, the neon isotope ratios indicate a mixture between atmospheric and MORB-type neon, most clearly visible in the gas from the 100m borehole (no. 111) and also for the Smrad'och mofette (no. 43) (Fig. 4). As mentioned earlier, the Dolní Častkov gas (no. 22) and that of the Prameny mineral spring (no. 38) may be weakly influenced by isotopic mass fractionation whereas the mofettes Soos (no. 26) and Mariiny (no. 46) were severely affected by mass fractionation. In contrast, the gas of the Františkový Lázně Mariin pramen (no. 110) could indicate admixture of nucleogenic (crustal) ^{21}Ne, which would be consistent with the only moderate $^{3}He/^{4}He$ ratio at this site compared with the high mantle-derived helium fractions at the degassing sites along the PPZ (Table 1).

The $^{40}Ar/^{36}$ data (Table 2) reflect mixing between atmospheric argon and a geogenic argon component. Most data lie close to the air $^{40}Ar/^{36}Ar$ ratio. The highest geogenic argon fractions were recorded in the two boreholes (nos. 111, 112), with nearly the same $^{40}Ar/^{36}Ar$ ratios in both boreholes of 30m and 100m depth, respectively. The $^{40}Ar/^{36}$ ratio in both the mantle and the crust is higher than in the atmosphere, but because of $^{3}He/^{4}He$ ratios close to the SCLM range and neon isotope ratios plotting on the air-MORB mixing line in Fig. 4, it is reasonable to suppose that the geogenic argon fraction at the locations along the PPZ consists of predominantly mantle-derived argon. This is consistent with the results of Bräuer et al. (2004), who studied $\delta^{15}N$ time-series data at the Bublák site in times of seismic quiescence, showing predominantly a two-component mixture between air and mantle-derived nitrogen.

5.2 Gas migration through clayey sediments

Due to its low permeability, argillaceous rock seems to be suitable as a geological barrier in radioactive waste disposal and for underground CO_2 storage (e.g. Horseman et al., 1999; Gerard et al., 2014). The initial reason for our gas monitoring in the clay pit (no. 91) was to use the natural degassing there as a critical analogue for the development and testing of monitoring techniques.

The clay pit is located somewhat west of the PPZ and directly to the north of the nature reserve Soos (Fig. 1, no. 91). Compared to the $^3He/^4He$ ratios of the Soos degassing sites (mean 3.4±0.1 R_a), those recorded in the clay pit (5.5±0.1 R_a, Table 3) are much closer to the SCLM range. In April 2006 a further increase of the $^3He/^4He$ ratios to 5.9 R_a was recorded (Table 3), contemporaneous with increased $^3He/^4He$ ratios lasting for three months at locations in the PPZ (Bräuer et al., 2009). The increase has been interpreted as indication for magma ascent associated with supply of fresh magma from a deeper reservoir. This finding suggests that the gases in the clay pit derive from the same magmatic reservoir that supplies the other degassing sites in the eastern part of the CB. In contrast to that, at the locations in the nature reserve Soos (no. 27) the $^3He/^4He$ level remained nearly constant (Fig. 11, Table 4, and Bräuer et al., 2009).

The data obtained monthly at the gas-rich site in the clay pit (Fig. 5) should reveal a possible influence of the seasonal cycle. If the gas composition follows a seasonal trend, the CO_2 concentration should correlate with the water temperature because the solubility of CO_2 in water depends strongly on the water temperature; the higher the water temperature, the higher the CO_2 fraction in the gas phase. Due to the large solubility differences between CO_2 and the non-acid gas components (e.g. helium, nitrogen) in water, helium should be inversely correlated. However, a clear trend induced by seasonal variations was not observed. Nevertheless, the helium and CO_2 concentrations as well as their isotope ratios did show some anomalies (Fig. 6). Two clear minima of the CO_2 concentration (<99 vol.%) were recorded along with the highest O_2 contents (Table 3). An increased fraction of dissolved air due to strong bubbling (Fig. 5 inset) may be responsible for these anomalies.

The $^3He/^4He$ ratios repeatedly showed values below the average (Table 3 marked by superscript a; Fig. 6). The mean of all recorded $^3He/^4He$ ratios at the site no. 91 is 5.54±0.14 R_a or, without the anomalies marked by a, b in Table 3, 5.59±0.06 R_a. The clay pit near Skalná is located close to the NK epicentral area (Fig. 1). Therefore, the helium isotope data may have been affected by the 2008 and 2011 earthquake swarms. The anomalies 1-3 (Fig. 6) may all have been generated by the 2008 swarm because seismically triggered admixture of crustal helium may occur repeatedly for two years after the onset of the swarm. This is shown by additional data from Bublák (no. 23) and Dolní Častkov (no. 22) given in Table 1, which continue the time series recorded in the aftermath of the 2008 swarm (Bräuer et al., 2014). Since 2000 more than 200 determinations of the $^3He/^4He$ ratio were obtained from the Bublák gas. Without seismically triggered anomalies (Bräuer et al., 2008, 2011, 2014), the mean is 5.92 ± 0.07 R_a. From the Dolní Častkov gas, more than 100 samples were taken, with a mean $^3He/^4He$ ratio of 5.15± 0.05 R_a (without seismically triggered anomalies). The latest helium anomaly was recorded in February 2011 in the Bublák gas and in October 2010 in the Dolní Častkov gas (Bräuer et al., 2014), i.e. within the same time frame as for anomalies 1-3 at the Skalná site. We can only speculate about the activating process of anomalies 4 and 5 (Fig. 6), which occurred prior to Aug. 2011, when the 2011 swarm started with a time difference of only 34 months after the onset of the 2008 swarm (Fischer et al., 2014; Fig. 6). However, also the Dolní Častkov and Bublák sites exhibit decreased $^3He/^4He$ ratios (Table 1) shortly before the beginning of the 2011 swarm. Such anomalies before the beginning of a seismically active period were already recorded before the 2000 earthquake swarm (Bräuer et al., 2008) and were explained by stress induced before fracturing takes place, resulting in the mobilization of small molecules (like He and H_2) also close to degassing sites and outside of the final rupture zone. Such a stress induced release of small molecules was also observed at other sites of seismic unrest, mostly in connection with magnitudes $M \geq 5$ (e.g. Sato et al., 1986) but also with magnitudes $M<3$ (e.g. Ito et al., 1999). The latest recorded anomalies (6 and 7 in Fig. 6) occurred after the beginning of the seismically active period 2011 and may have been generated by fracturing in the focal zone. Again, decreased $^3He/^4He$ ratios after the onset of the swarm were also recorded in the Dolní Častkov and Bublák gas (Table 1). No further anomalies were identified because the monthly sampling in the clay pit had to be terminated in December 2011 due to lack of further funding for the gas monitoring. In summary, the gases in the clay pit showed anomalies comparable to those observed at the degassing sites in the eastern part of the CB along the PPZ and the MLF during the investigation period (Bräuer et al., 2014).

Generally, clay is considered to act as a long term permeability barrier against the migration of fluids. But in addition to several N-S trending seismically active faults, e.g. the PPZ, Bankwitz et al. (2003) detected also a large ENE striking shear zone (Nová Ves fault, NVF) that was temporarily exposed in the clay pit Nová Ves II near Skalná. They described tiny channels of micrometer scale in the clay pit, which may serve as migration paths for the mantle-derived gases. Electron-microscopic studies of the clay indicate gas migration on vertical micro-tubes with diameters down to 1-2 μm (Bankwitz et al., 2003). The migration of gases with a high mantle-derived helium fraction on the NVF may indicate a deep-reaching fault structure.

5.3 The present geodynamical state in the investigation area

The hypocenters of the NK focal zone are mainly located at depths between 6.5 and 11 km. The largest recent swarms of 2000, 2008, and 2011 showed a progressively increasing speed of energy release connected with a decreasing duration of the main swarm period (Fischer et al., 2014). For the latest period of strong seismicity, starting in late May 2014, Hainzl et al.

(2016) distinguished three classical mainshock-aftershock sequences. Although no swarm-type seismicity was identified, the same focal zone as during earlier swarms was activated by 2014 events; therefore, the effect of the seismicity on the mantle-derived fluid flow signatures should be the same.

The 2000 swarm was accompanied by monitoring of gas and isotope compositions from May 2000 until December 2003. The period of seismicity starting in late August 2000 and lasting for four months caused anomalies of the $^3He/^4He$ ratios that occurred repeatedly over nearly two years (Bräuer et al., 2008). During strong swarm periods many seismic events (> 10,000) are recorded, generating fissures and resulting in the release of embedded crustal volatiles such as crustal helium. The released crustal volatiles migrate away from the focal zone, and when they encounter the steady fluid flow from the lithospheric mantle, they may be transported to the surface, modifying the helium signature for some time due to the clearly lower $^3He/^4He$ ratio of the admixed crustal helium.

Figure 3 illustrates the present contribution of mantle-derived helium (in relation to the SCLM signature; Gautheron et al., 2005) at locations which were first studied between 1992 and 1994 (Weinlich et al., 1999). At the locations marked in blue, the contribution of mantle-derived helium is clearly higher nowadays than 20 years ago, whereas in the ML degassing center and its surroundings no significant changes of the mantle-derived helium contributions are obvious. Besides that, it seems that the increase of mantle-derived helium is limited to the locations in the eastern part of the CB (Fig. 3, Table 4). Among the degassing locations in the CB and ML degassing centers that were repeatedly studied during the last 20 years (Bräuer et al., 2009), the mantle-derived helium fraction increased clearly at all studied locations in the CB with exception of the nature reserve Soos (no. 27) where the $^3He/^4He$ ratio remained nearly constant (Fig. 11, Table 4).

To the west of the nature reserve Soos, there are a lot of gas-rich mineral springs which are used for therapeutic treatments in the Františkovy Lázně spa. For this reason it was not possible to take samples repeatedly from the same sites for monitoring. In 2009 however, we could take samples from the mofette Mariin pramen in Františkovy Lázně for the first time (no. 110, Table 1). The contribution of mantle-derived helium at this site is similar to that in the nature reserve Soos. Although the gas flow and the CO_2 concentration are high at these degassing sites (Weinlich et al., 1999), they do not seem to be supplied by the same magmatic reservoir that supplies the locations in the eastern part of the CB and the degassing sites in the clay pit. This is suggested by the relatively low level of mantle-derived helium at the locations in Františkovy Lázně and the nature reserve Soos compared with those along the PPZ and because no indications for supply with fresh magma and/or magma intrusions in the crust were observed.

Gas studies in relation to periods of swarm earthquake activity repeatedly showed a decrease of the $^3He/^4He$ ratios at all studied locations in the CB (Bräuer et al., 2008; 2011; 2014). The $^3He/^4He$ ratios from the sampling campaign 2015 confirmed these findings (Fig. 11, Table 1). In a borehole (no. 112 in Table 1) belonging to the Hartoušov mofette field close to the PPZ, Fischer et al. (2017) observed a fast increase of the gas flow up to six times the average, contemporaneously with the beginning of the seismically active period 2014, whereas simultaneously the gas flow at the Dolní Částkov site (no. 22) on the MLF declined towards zero and only returned to the normal level in 2016, implying different permeability changes of the migration paths in the PPZ and the MLF caused by seismic activity.

During the timespan of our gas studies, four periods of strong seismicity with magnitudes >3 occurred in the NK focal zone in NW Bohemia in 2000, 2008, 2011 (Fischer et al., 2014), and 2014 (Hainzl et al., 2016). Before that, the last period when such clusters of relatively strong earthquake swarms had been observed was between 1897 and 1908. Neunhöfer and Hemmann (2005) estimated the maximum magnitude to ML≈4.4 for the sequence of swarms between 1897 and 1908. Thereafter, the recorded seismicity was weaker. Prior to the strong earthquake swarm in 1985/86 with ML_{max}=4.6, the recorded magnitudes were <3 (Neunhöfer and Hemmann, 2005).

Figure 11 shows that $^3He/^4He$ ratios > 6 R_a were observed before the 2000 and also before the 2008 swarm at locations along the PPZ, indicating the supply of fresh, less degassed magma from a deeper reservoir and/or the occurrence of small magma intrusions in the crust (Bräuer et al., 2009). The Bublák site acts still as a deep-seated injection zone of mantle-derived gases (Bräuer et al., 2011) that supplies the locations in the eastern part of the CB on the N-S trending faults (PPZ, MLF) and the ENE trending fault zone (NVF) with fluids from the SCLM. Since May 2000, the helium isotope ratios of the Bublák gas lie within the SCLM range, followed by a further increase. Since 2005, the contribution of mantle-derived helium has been permanently higher than in 1993 at all studied locations in the eastern part of the CB (Fig. 11). Future studies will show whether, like after the strong period of seismicity between 1897 and 1908, again a longer period of weak seismicity will follow, and whether the $^3He/^4He$ ratios will remain at the high present level in the CB.

Conclusion

In the ECRIS there are only few locations where free gases with plain SCLM signature escape at the surface. Gases from the SCLM can only retain their signature to a large extent when they are transported on a highly permeable migration path reaching down to the SCLM. In the western Eger Rift area, only the gas from locations along the PPZ retains the SCLM signature. According to the time-series data (1994 to 2016), an ongoing hidden magmatic process is indicated beneath this area only. The gas signature of the Bublák gas is similar to that of the fresh magmatic gas sampled during an eruptive episode of Oldoinyo Lengai located in the western part of the East African Rift Valley.

The latest studies in the western Eger Rift confirmed the different contributions of mantle-derived helium in the degassing centers and that the increase of the mantle-derived helium fraction is limited to the degassing sites in the eastern part of the Cheb Basin. At mofettes along the PPZ, also mantle-derived neon, argon and nitrogen fractions are indicated. As a whole, gases from mofette-type degassing sites are less affected by fractionation processes near the surface.

The detailed characterization of the gas migration in the clay pit between 2001 and 2014 has confirmed the E-W striking fault (NFV) first reported by Bankwitz et al. (2003).

Changes of the gas signatures triggered by seismicity occurring in the NK focal zone were only observed within the CB and its periphery so far. Decreased $^{3}He/^{4}He$ ratios due to the seismically active period 2014 were observed at locations along the PPZ, the MLF and the NFV (clay pit). The permeability of the migration paths connecting the focal zone with the steady mantle-derived fluid flow and the distance to the respective degassing sites determine when such seismically triggered anomalies may occur.

When off-line sampling procedures are applied, it depends on the timing of the sampling how many anomalies can be identified. Nevertheless, the existing data indicate anomalies occurring at different times on different faults, but to confirm this statement, online measurements would be required. Unfortunately, it is too difficult or requires an enormous expenditure to record the gas composition and the isotope ratios (He, Ne, Ar, C, N) online. Nonetheless, for evaluating geodynamic processes and their timescales, a long-term monitoring strategy is desirable.

Acknowledgement

For support at sampling sites in spas the authors would like to thank T. Vylita and J. Tesař. T. Fischer and T. Vylita are acknowledged for support with sampling at boreholes in the Hartoušov mofette field and at Dolní Častkov. We thank the company LB Minerals for giving permission to take samples in the clay pit Nová Ves II and especially M. Zikmund for supporting our work within the clay pit.

The authors would also like to thank J. Sültenfuß (University of Bremen, Institute of Environmental Physics) for the $^3He/^4He$ ratio measurements, J. Tesař (Laborunion CZ, Františkovy Lázně) for the gas composition measurements, and E. Schnabel for noble gas analyses at GFZ Potsdam. Technical assistance was provided by W. Städter. The project was kindly funded by the German Science Foundation (BR 1396/7). The comments by two anonymous reviewers is gratefully acknowledged.

References

Aeschbach-Hertig, W., Kipfer, R., Hofer, M., Imboden, D. M., Wieler, R., Signer, P., 1996. Quantification of gas fluxes from the subcontinental mantle: The example of Laacher See, a maar lake in Germany. Geochim. Cosmochim. Acta 60, 31-41.

Babuška, V., Plomerová, J., Fischer, T., 2007. Intraplate seismicity in the western Bohemian Massif (central Europe): A possible correlation with a paleoplate junction. J. Geodyn. 44, 149-159.

Ballentine, C.J., 1997. Resolving the mantle He/Ne and crustal $^{21}Ne/^{22}Ne$ in well gases. Earth Planet. Sci. Lett. 152, 233-249.

Ballentine, C.J, O'Nions, R.K., Oxburgh, E.R., Horvath, F., Deak, J., 1991. Rare gas constraints on hydrocarbon accumulation, crustal degassing and groundwater flow in the Pannonian basin. Earth Planet. Sci. Lett. 105, 229-246.

Bankwitz, P., Schneider, G., Kämpf, H., Bankwitz, E., 2003. Structural characteristics of epicentral areas in central Europe (Czech Republic). J. Geodyn. 35, 5-32.

Barry, P.H., Hilton, D.R., Fischer, T.P., de Moor, J.M., Mangasini, F., Ramirez, C., 2013. Helium and carbon isotope systematics of cold "mazuku" CO_2 vents and hydrothermal gases and fluids from Rungwe Volcanic Province, southern Tanzania. Chem. Geol. 339, 141-156.

Battani, A., Deville, E., Faure, J.L., Noirez, S., Tocqué, E., Benoît, Y., Schmitz, J., Parlouar, D., Sarda, P., Gal, F., Le Pierres, K., Brach, M., Braibant, G., Beny, C., Pokryszka, Z., Charmoille, A., Bentivegna, G., Pironon, J., de Donato, P., Garnier, C., Cailteau, C., Barrès, O., Radilla, G., Bauer, A., 2010. Geochemical study of natural CO_2 emissions in the French Massif Central: How to predict origin, processes and evolution of CO_2 leakage. Oil & Gas Science and Technology – Rev., IFP, 615-633.

Bräuer, K., Kämpf, H., Strauch, G., Weise, S.M., 2003. Isotopic evidence ($^3He/^4He$, $^{13}C_{CO2}$) of fluid triggered intraplate seismicity. J. Geophys. Res. 108, doi:10.1029/2002JB002077.

Bräuer, K., Kämpf, H., Niedermann, S., Strauch, G., Weise S.M., 2004. Evidence for a nitrogen flux directly derived from the European subcontinental mantle in the Western Eger Rift, central Europe. Geochim. Cosmochim. Acta 68, 4935-4947.

Bräuer, K. Kämpf, H., Faber, E. Koch, U., Nitzsche, H.-M., Strauch, G., 2005a. Seismically triggered microbial methane production relating to the Vogtland-NW Bohemia earthquake swarm period 2000, Central Europe. Geochem. J. 39, 441-450.

Bräuer, K., Kämpf, H., Niedermann, S., Strauch, G., 2005b. Evidence for ascending upper mantle-derived melt beneath the Cheb Basin, central Europe. Geophys. Res. Lett. 32, L08303, doi:10.1029/2004GL022205.

Bräuer, K., Kämpf, H., Niedermann, S., Strauch, G., Tesař, J., 2008. The natural laboratory NW Bohemia – Comprehensive fluid studies between 1992 and 2005 used to trace geodynamic processes. Geochem. Geophys. Geosys. 9, Q04018, doi: 10.1029/2007GC001921.

Bräuer, K., Kämpf, H., Strauch, G., 2009. Earthquake swarms in non-volcanic regions: What fluids have to say. Geophys. Res. Lett. 36, L17309, doi: 10.1029/2009GL039615.

Bräuer, K., Kämpf, H., Koch, U., Strauch, G., 2011. Monthly monitoring of gas and isotope composition in the free gas phase at degassing locations close to the Nový Kostel focal zone in the western Eger Rift, Czech Republic. Chem. Geol. 290, 163-173.

Bräuer, K., Kämpf, H., Niedermann, S., Strauch, G., 2013. Indications for the existence of different magmatic reservoirs beneath the Eifel area (Germany): A multi-isotope (C, N, He, Ne, Ar) approach. Chem. Geol. 356, 193-208.

Bräuer, K., Kämpf, H., Strauch, G., 2014. Seismically triggered anomalies in the isotope signatures of mantle-derived gases detected at degassing sites along two neighboring faults in NW Bohemia, central Europe. J. Geophys. Res. Solid Earth 119, 5613–5632.

Bräuer, K., Kämpf, H., Niedermann, S., Wetzel, H.-U., 2017. Regional distribution pattern of carbon and helium isotopes from different volcanic fields in the French Massif Central: Evidence for active mantle degassing and water transport. Chem. Geol. 469, 4-18. http://dx.doi.org/10.1016/j.chemgeo.2017.04004.

Caracausi, A., Italiano, F., Martinelli, G., Paonita, A., Rizzo, A., 2005. Long-term geochemical monitoring and extensive/compressive phenomena: case study of the Umbria Region (Central Apennines, Italy). Ann. Geophys. 48, 43-53.

Chiodini, G., Caliro, S., Cardellini, C., Granieri, D., Baldini, A., Donnini, M., Minopoli, C., 2010. Long-term variations of the Campi Flegrei, Italy, volcanic system as revealed by the monitoring of hydrothermal activity. J. Geophys. Res. 115, B03205, doi: 10.1029./2008JB006258.

Chiodini, G., Caliro, S., Cardellini, C., Frondini, F., Inguaggiato, S., Matteucci, F., 2011. Geochemical evidence for and charaterization of CO_2 rich gas sources in the epicentral area of the Abruzzo 2009 earthquakes. Earth Planet. Sci. Lett. 304, 389-398.

de Leeuw, G.A.M., Hilton, D.R., Güleç, N., Mutlu, H., 2010. Regional and temporal variations in $CO_2/^3He$, $^3He/^4He$ and $\delta^{13}C$ along the North Anatolian Fault Zone, Turkey. Appl. Geochem. 25, 524-539.

de Mohr, J.M., Fischer, T.P., Sharp, Z.D., Hilton, D.R., Barry, P.H., Mangasini, F., Ramirez, C., 2013. Gas chemistry and nitrogen isotope composition of cold mantle gases from Rungwe Volcanic Province, southern Tanzania. Chem. Geol. 339, 30-42.

Dunai, T.J., Porcelli, D., 2002. Storage and transport of noble gases in the subcontinental lithosphere. Reviews in Mineralogy & Geochemistry 47, 371-409.

Eichelberger, J.C., Vogel, T.A., Younker, L.W., Miller C.D., Heiken, G.H., Wohletz, K.H., 1988. Structure and stratigraphy beneath a young phreatic vent: South Inyo Crater, Long Valley Caldera, California. J. Geophys. Res. 93, B11, 13,208-13,220.

Fischer, T., Horálek, J., 2003. Space-time distribution of earthquake swarms in the principal focal zone of the NW-Bohemian/Vogtland seismoactive region: period 1985-2001. J. Geodyn. 35, 125-144.

Fischer, T., Horálek, J., Michálek, J., Boušková, A., 2010. The 2008 West Bohemia earthquake swarm in the light of the WEBNET network. J. Seismol. 14, 665 -682.

Fischer, T., Horálek, J., Hrubcová, P., Vavryčuk, V., Bräuer, K., Kämpf, H., 2014. Intra-continental earthquake swarms in West-Bohemia and Vogtland: A review. Tectonophys. 611, 1-27.

Fischer, T., Matyska, C., Heinicke, J., 2017. Earthquake enhanced permeability – evidence from carbon dioxide release following the M_L 3.5 earthquake in West Bohemia. Earth Planet. Sci. Lett. 460, 60-67.

Fischer, T.P., Giggenbach, W.F., Sano, Y., Williams, S.N., 1998. Fluxes and sources of volatiles discharged from Kudryavy, a subduction zone volcano, Kurile Islands. Earth Planet. Sci. Lett. 160, 81-96.

Fischer, T.P., Burnard; P., Marty, B., Hilton, D.R., Füri; E., Palhol, F., Sharp, Z.D., Mangasini, F., 2009, Upper-mantle volatile chemistry at Oldoinyo lengai volcano and the origin of carbonatites. Nature 459, 77-80.

Gautheron, C., Moreira, M., Allègre, C., 2005. He, Ne and Ar composition of the European lithospheric mantle. Chem. Geol. 217, 97-112.

Geissler, W.H., Kämpf, H., Kind, R., Bräuer, K., Klinge, K., Plenefisch, T., Horalek, J., Zednik, J., Nehybka, V., 2005. Seismic structure and location of a CO_2 source in the upper mantle of the western Eger (Ohre) Rift, central Europe. Tectonics 24, TC5001, doi:10.1029/2004TC001672.

Gerard, P., Harrington, J., Charlier, R., Collin, F., 2014. Modelling of localised gas preferential pathways in claystone. International Journal of Rock Mechanics & Mining Sciences, 67, 104-114.

Griesshaber, E., O'Nions, R.K., Oxburgh, E.R., 1992. Helium and carbon isotope systematics in crustal fluids from the Eifel, the Rhine Graben and Black Forest, F.R.G. Chem. Geol. 99, 213-235.

Grünthal, G., Schenk, V., Zeman, A., Schenková, A., 1990. Seismotectonic model for the earthquake swarm of 1985-1986 in the Vogtland/West Bohemia focal area. Tectonophys. 174, 369-383.

Hainzl, S., Fischer, T**.,** Čermáková H**.,** Bachura**,** M., Vlček, J., 2016. Aftershocks triggered by fluid intrusion: Evidence for the aftershock sequence occurred 2014 in West Bohemia/Vogtland. J. Geophys. Res. Solid Earth, 121, 2575-2590.

Heuer, B., Geissler,W.H., Kind, R., Kämpf, H., 2006. Seismic evidence for asthenospheric updoming beneath the western Bohemian Massif, Central Europe. Geophys. Res. Lett. 33, L05311, doi:10.1029/2005Gl025158.

Heuer, B., Geissler, W.H., Kind, R., the BOHEMA working group, 2011. Receiver function search for a baby plume in the mantle transition zone beneath the Bohemian Massif. Geophys. J. Int. 187, 577–594.

Hill, D.P., 1977. A model for earthquake swarms, J. Geophys. Res. 82, 1347-1352.

Hill, D.P., Prejean, S., 2005. Magmatic unrest beneath Mammoth Mountain, California, J. Volcan. Geotherm. Res. 146, 257-283.

Hilton, D.R., 1996. The helium and carbon isotope systematicsof a continental geothermal system: results from monitoring studies at Long Valley Caldera (California, U.S.A.). Chem. Geol. 127, 269-295.

Hilton, D.R., Halldórsson, S.A., Barry, P.H., Fischer, T.P., de Moor, J.M., Ramirez, C.J., Mangasini, F., Scarsi, P., 2011. Helium isotopes at Rungwe Volcanic Province, Tanzania, and the origin of East African Plateaux. Geophys. Res. Lett. 38, L21304, doi: 10.1029/2011GL049589.

Hinzen, K.-G., 2003. Stress field in the northern Rhine area, Central Europe, from earthquake fault plain solutions. Tectonophys. 377, 325-356.

Honda, M., McDougall, I., Patterson, D.B., Doulgeris, A., Clague, D.A., 1991. Possible solar noble-gas component in Hawaiian basalts. Nature 349, 149-151.

Horseman, S.T., Harrington, J.F., Sellin, P., 1999. Gas migration in clay barriers. Engineering Geology 54, 139–149.

Hrubcová, P., Geissler, W.H., 2009. The Crust-Mantle Transition and the Moho beneath the Vogtland/West Bohemian Region in the light of different seismic methods. Stud. Geophys. Geod. 53, 275-294.

Hrubcová, P., Vavryčuk, V., Boušková, A., Horálek, J., 2013. Moho depth determination from waveforms of microearthquakes in the West Bohemia/Vogtland swarm area. J. Geophys. Res. 118, 1–17.

Hrubcová, P., Geissler, W.H., Bräuer, K., Vavryčuk, V., Tomek, Č., Kämpf, H., 2017. Active magmatic underplating in western Eger Rift, Central Europe. Tectonics 36. https://doi.org/10.1002/2017TC004710.

Ibs-von Seht, M., Plenefisch, T., Klinge, K., 2008. Earthquake swarms in continental rifts – A comparison of selected cases in America, Africa and Europe. Tectonophys. 452, 66-77.

Ito, T., Nagamine, K., Yamamotu, K., Adachi, M., Kawabe, I., 1999. Preseismic hydrogen gas anomalies caused by stress-corrosion preceding earthquakes. Geophys. Res. Lett. 26, 2009-2012.

Javoy, M., Pineau, F., 1991. The volatiles record of a “popping” rock from Mid-Atlantic Ridge at 14°N: chemical and isotope composition of gas trapped in the vesicles. Earth Planet. Sci. Lett. 107, 598-611.

Kämpf, H., Bräuer, K., Schuhmann, J., Hahne, K., Strauch, G., 2013. CO_2 discharge in an active non-volcanic continental rift area (Czech Republic): Characterization ($\delta^{13}C$, $^3He/^4He$) and quantification of diffuse and vent CO_2 emissions. Chem. Geol. 339, 71-83.

Kennedy, B.M., Hiyagon, H., Reynolds, J.H., 1990. Crustal neon: a striking uniformity. Earth Planet. Sci. Lett. 98, 277-286.

Kipfer, R., Aeschbach-Hertig, W., Peeters, F., Stute, M., 2002. Noble gases in lakes and ground waters. Reviews in Mineralogy & Geochemistry 47, 615-700.

Lee, H.-F., Yang, T.F., Lan, T.F., Chen, C.-H., Song, S.-R., Tsao, S., 2008. Temporal variations of the gas compositions of fumaroles in the Tatun Volcano Group, northern Taiwan. J. Volcan. Geotherm. Res. 178, 624-635.

Martelli, M., Caracausi, A., Paonita, A., Rizzo, A., 2008. Geochemical variations of air-free crater fumaroles at Mt. Etna: New inferences for forecasting shallow volcanic activity. Geophys. Res Lett. 35, L21302, doi: 10.1029/2008GL035118.

Matthews, A., Fouillac, C., Hill, R., O’Nions, R.K., Oxburgh, E.R., 1987. Mantle-derived volatiles in continental crust: the Massif Central of France. Earth Planet. Sci. Lett. 85, 117-128.

Mazabraud, Y., Béthoux, N., Guilbert, J., Bellier, O., 2005. Characterisation of the seismological pattern in a slowly deforming intraplate region: central and western France. Tectonophys. 409, 175–192.

Mrlina, J., Kämpf, H., Kroner, C., Mingram, J., Stebich, M., Brauer, A., Geissler, W.H., Kallmeyer, J., Matthes, H., Seidl, M., 2009. Discovery of the first Quaternary maar in the Bohemian Massif, Central Europe, based on combined geophysical and geological surveys. J. Volcan. Geotherm. Res. 182, 97-112.

Neunhöfer, H., Hemmann, A., 2005. Earthquake swarms in the Vogtland/Western Bohemia region: Spatial distribution and magnitude–frequency distribution as an indication of the genesis of swarms? J. Geodyn. 39, 361-385.

Niedermann, S., Bach, W., Erzinger, J., 1997. Noble gas evidence for a lower mantle component in MORBs from the southern East Pacific Rise: Decoupling of helium and neon isotope systematics. Geochim. Cosmochim. Acta 61, 2697-2715.

Pačes, T., 1974. Springs of carbon-dioxide waters in northwestern Bohemia. In:Field-trip Guide. Proc. Intern. Symp. Water-Rock Interaction Prague 1974. UUG (Czech Geol. Survey) Prague.

Pačes, T., 1987. Hydrochemical evolution of saline waters from crystalline rocks of the Bohemian Massif (Czechoslovakia). In: Saline water and gases in crystalline rocks (eds P. Fritz and S.K. Frape). Geol. Assoc. Canad. Spec. Pap. 33, pp.145-156.

Rohrmüller, J., Kämpf,H., Geiß, E., Großmann, J., Grun, I., Mingram, J., Mrlina, J., Plessen, B., Stebich, M., Veress, C., Wendt, A., Nowaczyk, N., 2017. Reconnaissance study of an inferred Quaternary maar structure in the western part of the Bohemian Massif near Neualbenreuth, NE-Bavaria (Germany). Submitted to International Journal of Earth Sciences.

Sano, Y., Marty, B., 1995. Origin of carbon in fumarolic gas from island arcs. Chem. Geol. 119, 265-274.

Sano, Y., Takahata, N., Igarashi, G., Koizumi, N., Sturchio, N.C., 1998. Helium degassing related to the Kobe earthquake. Chem. Geol. 150, 171-179.

Sarda, P., Staudacher, T., Allègre, C.J., 1988. Neon isotopes in submarine basalts. Earth Planet. Sci. Lett. 91, 73-88.

Sato, M., Sutton, A.J., McGee, K.A., Russel-Robinson, S., 1986. Monitoring of hydrogen along the San Andreas and Calaveras Faults in central California in 1980-1984. J. Geophys. Res. 91, 12,315-12,326.

Schlindwein, V., 2012. Teleseismic earthquake swarms at ultraslow spreading ridges: indicator for dyke intrusions? Geophys. J. Int. 190, 442-456.

Sigmundsson, F., Einarsson, P., Rögnvaldsson, S.T., Foulger, G.R., Hodgkinson, K.M., Thorbergsson G., 1997. The 1994-1995 seismicity and deformation at the Hengill triple junction, Iceland: Triggering of earthquakes by minor magma injection in a zone of horizontal shear stress. J. Geophys. Res. 102, 15,151-15,161.

Snyder, G., Poreda, R., Hunt, A., Fehn, U., 2001. Regional variations in volatile composition: Isotopic evidence for carbonate recycling in the Central American volcanic arc. Geochem. Geophys. Geosyst. 2, doi: 2001GC000163.

Sugisaki, R., Sugiura, T., 1986. Gas anomalies at three mineral springs and a fumarole before an inland earthquake, central Japan. J. Geophys. Res. 91, 12,296-12,304.

Sültenfuß, J., Rhein, M., Roether W., 2009. The Bremen Mass Spectrometric Facility for the measurement of heliumisotopes, neon, and tritium in water. Isotopes Environ. Health Stud. 45, 1-13.

Toutain, J.P., Baubron J.-C., 1999. Gasgeochemistry and seismotectonics: a review, Tectonophys. 304, 1-27.

van Soest, M.C., Hilton, D.R., Kreulen, R., 1998. Tracing crustal and slab contributions to arc magmatism in the Lesser Antilles island arc using helium and carbon relationships in geothermal fluids. Geochim. Cosmochim. Acta 62, 3323-3335.

Vaselli, O., Tassi, F., Duarte, E., Fernandez, E., Poreda, R.J., Delgato Huertas, A. 2010. Evolution of fluid geochemistry at the Turrialba volcano (Costa Rica) from 1998 to 2008. Bull. Volcanol. 72, 397-410.

Weinlich, F.H., Tesař, J., Weise, S.M., Bräuer, K., Kämpf H., 1998. Gas flux contribution in mineral springs and tectonic structure in the western Eger Rift. J. Czech Geol. Soc. 43, 91-110.

Weinlich, F.H., Bräuer, K., Kämpf, H., Strauch, G., Tesař, J., Weise, S.M., 1999. An active subcontinental mantle volatile system in the western Eger Rift, Central Europe: Gas flux, isotopic (He, C, N) and compositional fingerprints. Geochim. Cosmochim. Acta 63, 3653-3671.

Werner, C., Evans, W.C., Poland, M., Tucker, D.S., Douklas, M.P., 2009. Long-term changes in quiescent degassing at Mount Baker Volcano, Washington, USA; Evidence for a stalled intrusion in 1975 and connection to a deep magma source. J. Volcan. Geotherm. Res. 186, 379-386.

Zartman, R.E., Wasserburg, G.J., Reynolds, J. H., 1961. Helium, argon, and carbon in some natural gases. J. Geophys. Res. 66, 277-291.

Ziegler, P.A., 1992. European Cenozoic rift system. Tectonophys. 208, 91-111.

Figure captions

Fig. 1 Topographical map (modified after Hrubcová et al., 2017) showing the investigation area in the Czech/German border region. The white circles indicate all degassing sites which were studied (numbers according to Weinlich et al., 1999; Geissler et al., 2005). The yellow circle marks the position of the degassing site in the clay pit near Skalná, where monthly monitoring of the gas and isotopic compositions was carried out. Three degassing centers are indicated by black dashed circles (CB, Cheb Basin; ML, Mariánské Lázně; KV, Karlovy Vary). Seismic events are marked by small red dots which are concentrated in the Nový Kostel (NK) focal zone. The major fault zones Eger Rift (ER), Mariánské Lázně Fault (MLF), Tachov Fault (TF), and Počatky-Plesná Zone (PPZ) as well as four Quaternary volcanoes are indicated (KH, Komorní hůrka; ZH, Železná hůrka; MM, Mýtina Maar; NM, Neualbenreuth Maar). KTB denotes the site of the German Continental Deep Drilling Program. The inset shows the position of the investigation area in Central Europe. Numbers and names of sampling sites are listed in Table 1.

Fig. 2 Relative N_2-He-Ar abundances in free gas; (a) data from CB sites, (b) data from ML, KV and surroundings. The gray triangle marks the range for mantle origin. The black squares correspond to air and air-saturated water (ASW; Kipfer et al., 2002). Classification of subduction-derived gases after Fischer et al. (1998). Numbers and names of sampling sites are listed in Table 1.

Fig. 3 Regional distribution pattern of mantle helium contributions and $\delta^{13}C$ values (small negative italic numbers) plotted on the topographical map. The black or blue sectors correspond to the fraction of helium derived from the SCLM, assuming $(^3He/^4He)_{SCLM}$ = 6.32 R_a (Gautheron et al., 2005). At the locations shown by black sectors, the fraction of SCLM helium has remained nearly the same since the first characterization between 1992 and 1994 (Weinlich et al., 1999), whereas the locations marked by blue sectors showed an increase of SCLM helium fractions since the first study. Bigger black numbers denote sampling sites. Numbers and names of sampling sites are listed in Tables 1 and 4. See Fig. 1 for abbreviations.

Fig. 4 Neon three-isotope plot showing the data of all sites studied for Ne. Uncertainties are 2σ. For reference, the air composition, the mass fractionation line (mfl), the Loihi-Kilauea (L-K) line (air-plume mixing; Honda et al., 1991), the MORB line (air-MORB mixing; Sarda et al., 1988), and the Continental crust line (Kennedy et al., 1990) are given. Numbers and names of sampling sites are listed in Table 1.

Fig. 5 Photo gives a view of the clay pit Nová Ves II near Skalná (location no. 91) and the inset shows the sampling site of the time-series data in more detail.

Fig. 6 Temporal variations of (a) $^3He/^4He$ ratios and $\delta^{13}C$ values and (b) He and CO_2 concentrations at the degassing site in the clay pit Nová Ves II near Skalná. In (a), the mean $^3He/^4He$ ratio without anomalies (5.59±0.06 R_a) and in (b), the water temperature are also shown.

Fig. 7 $^3He/^4He$ vs. $^4He/^{20}Ne$ plot. The curves represent mixing between air and SCLM or crust, respectively. In addition, the Escarot data is plotted for reference (Bräuer et al., 2017); at that degassing site in the French Massif Central, which belongs to the ECRIS also, the highest $^3He/^4He$ ratios were recorded. The $^3He/^4He$ ratios in this plot are not corrected for the atmospheric He contribution. Numbers and names of sampling sites are listed in Table 1.

Fig. 8 $^3He/^4He$ vs. $CO_2/^3He$ ratios of the sampled gases in relation to a binary mixing model between a hypothetical SCLM endmember with a fixed composition ($^3He/^4He$=6.32Ra; $CO_2/^3He=2x10^9$) and various crustal endmembers with $^3He/^4He$=0.02 Ra and different $CO_2/^3He$ ratios. The $^3He/^4He$ range for the European SCLM was used (Gautheron et al., 2005). The range of SCLM $CO_2/^3He$ ratios (Dunai and Porcelli, 2002) is not well constrained (see text). Therefore, as reference again the Escarot data (Bräuer et al., 2017) were used. Panel (a) shows the CB data and (b) the data from ML, KV and surroundings. $^3He/^4He$ ratios corrected for air contamination using the He/Ne ratios were used here. Numbers and names of sampling sites are listed in Table 1.

Fig. 9 (a) Diagram showing the inverse correlation between $CO_2/^3He$ ratios and helium concentrations. Again as reference for SCLM origin, the Escarot data (Bräuer et al., 2017) is shown. The dashed line is a linear regression line (r^2=0.988). Numbers and names of sampling sites are listed in Table 1. (b) $CO_2/^3He$ vs. $\delta^{13}C$ diagram shows the $\delta^{13}C$ value of the gases in relation with mixing lines between the SCLM (Escarot: $\delta^{13}C$=-3.6‰ and $CO_2/^3He$ =4.2 10^9 after Bräuer et al., 2017) and organic carbon (S:

$\delta^{13}C$=-30‰ and $CO_2/^3He$ = 10^{13}) or limestone (L: $\delta^{13}C$=0‰ and $CO_2/^3He$ = 10^{13}), respectively (Sano and Marty, 1995).

Fig. 10 Ternary CO_2-^3He-^4He plot. Plot (a) shows the CB data and (b) the data from ML, KV and surroundings. As reference for the SCLM the Escarot data (Bräuer at al., 2017) is additionally plotted. Popping rock data is given as reference for MORB (Javoy and Pineau, 1991). The arrows indicate processes that may have modified the signatures. Numbers and names of sampling sites are listed in Table 1.

Fig. 11 Variations of $^3He/^4He$ ratios at various degassing locations in the Cheb Basin between 1993 and 2016. The error bars are smaller than the symbols. The red symbols correspond to locations at which the fraction of mantle-derived helium has increased since 1993. The green squares show data from the Cisařský pramen in the nature reserve Soos (no. 27), a location west of the fault zones (PPZ and MLF) with nearly constant $^3He/^4He$ ratios. The SCLM range is given by xenolith studies (Gautheron et al., 2005). Two black arrows indicate supply of fresh, less degassed magma due to an ongoing hidden magmatic process beneath the Cheb Basin. The red arrows below point to the beginning of four earthquake swarms (EQS; M_L> 3) which occurred during the fluid studies.

Figure
Click here to download high resolution image

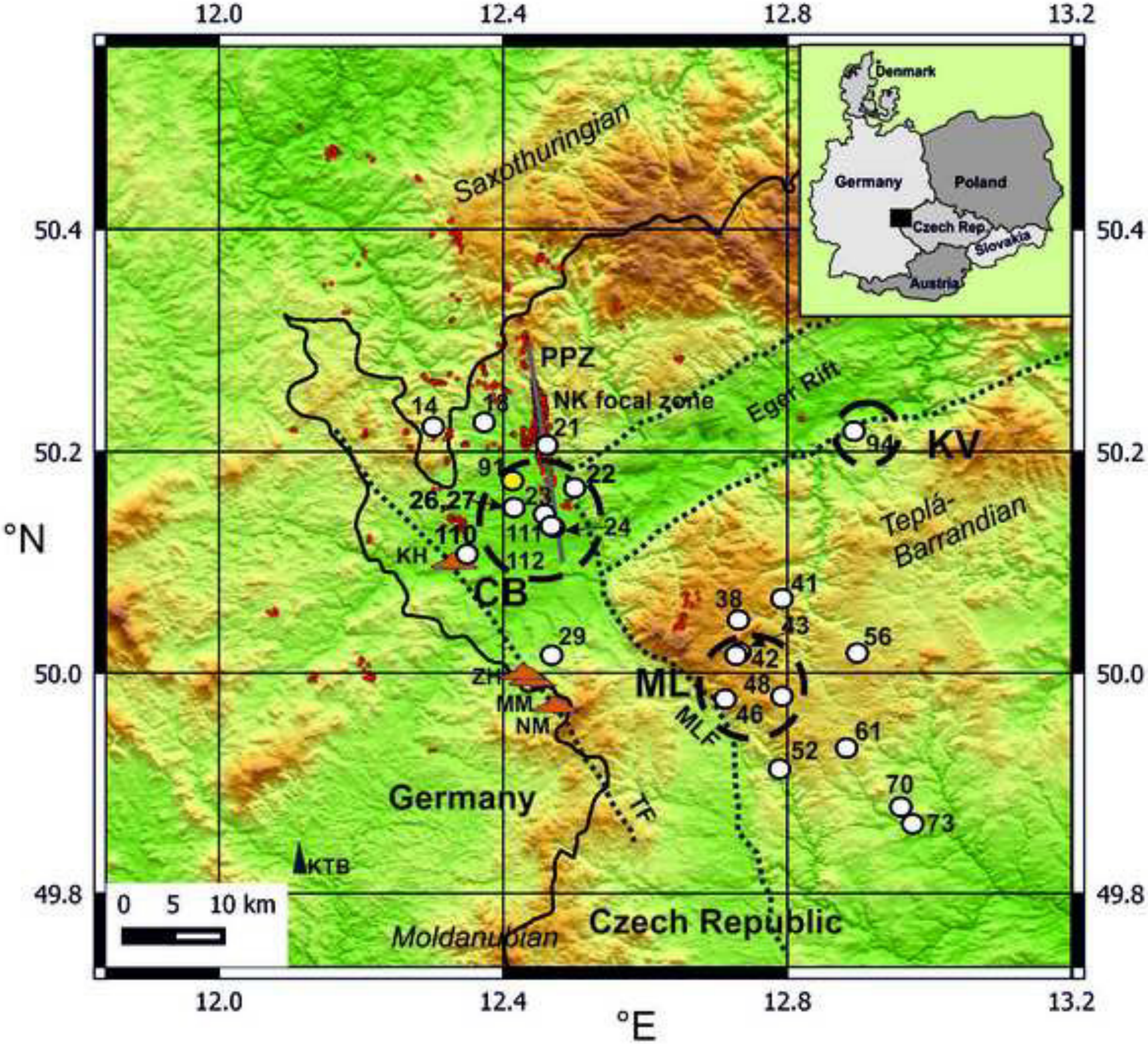

Figure
Click here to download high resolution image

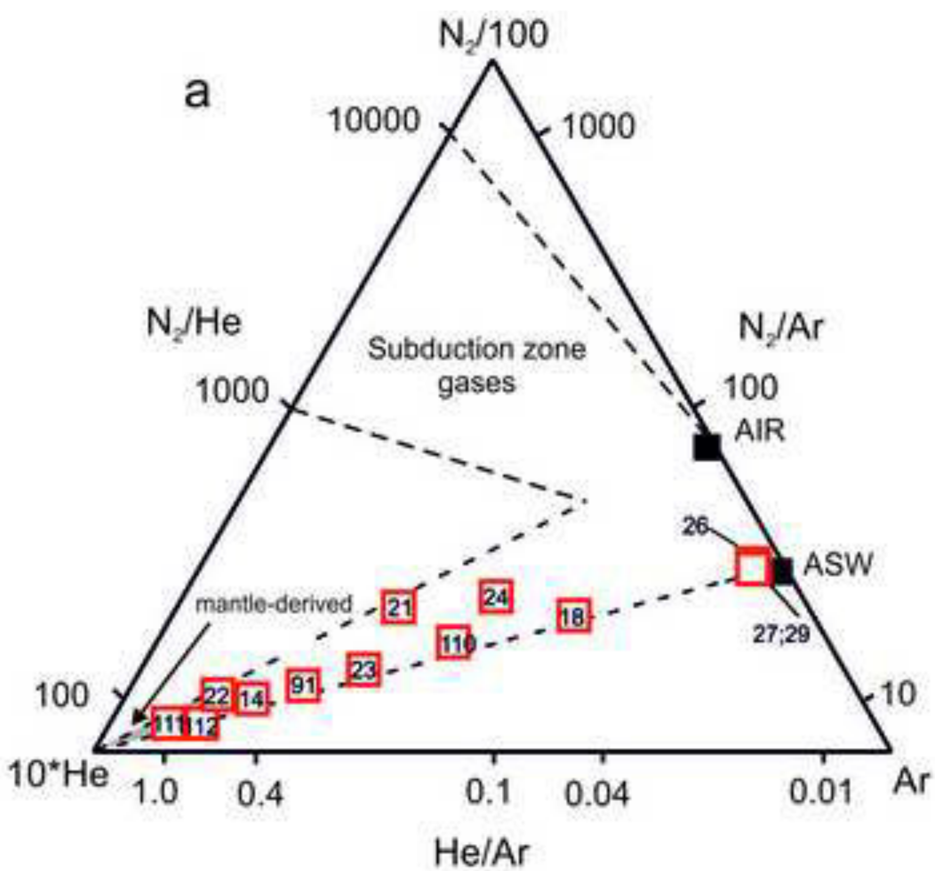

Figure
Click here to download high resolution image

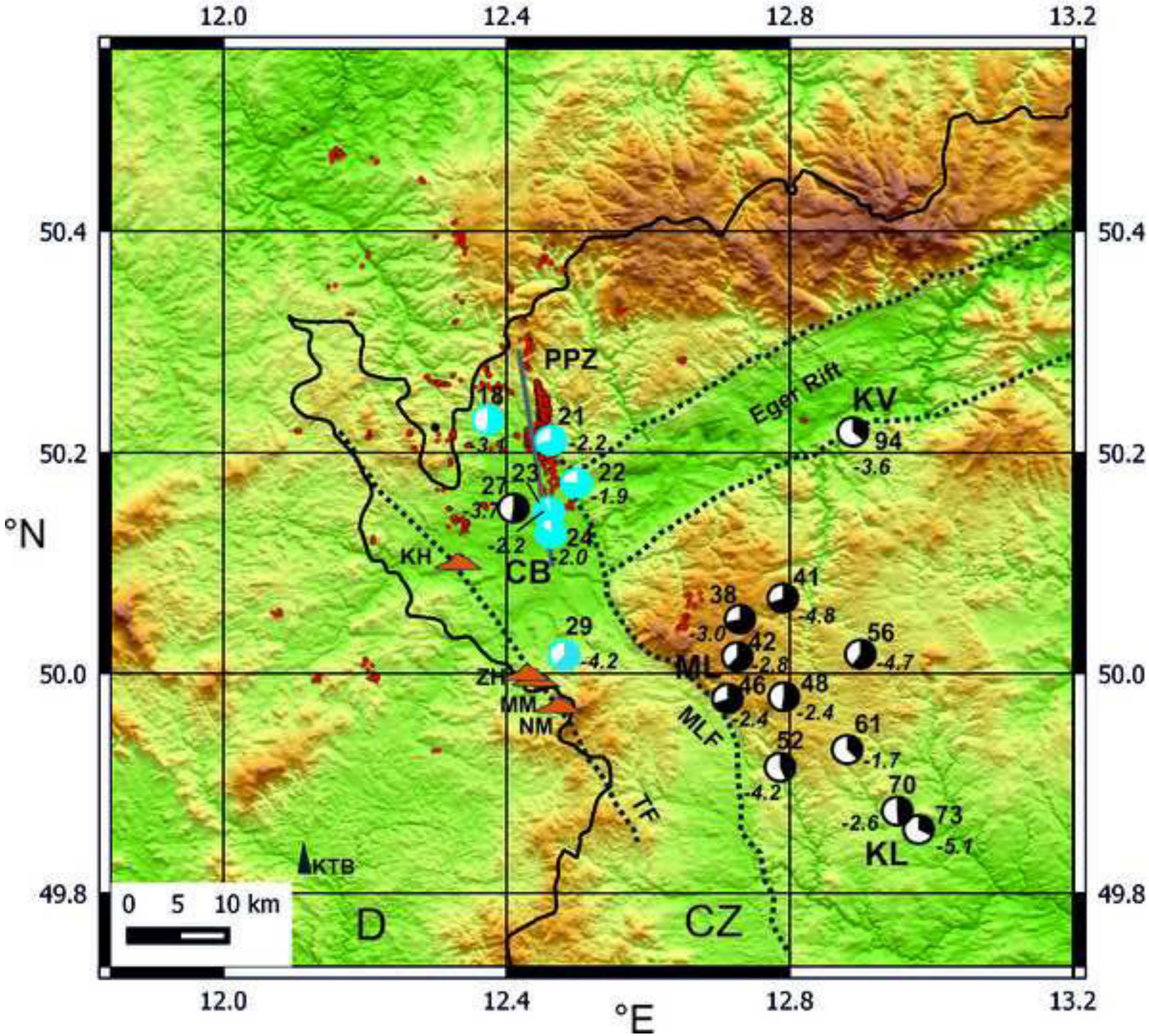

Figure
Click here to download high resolution image

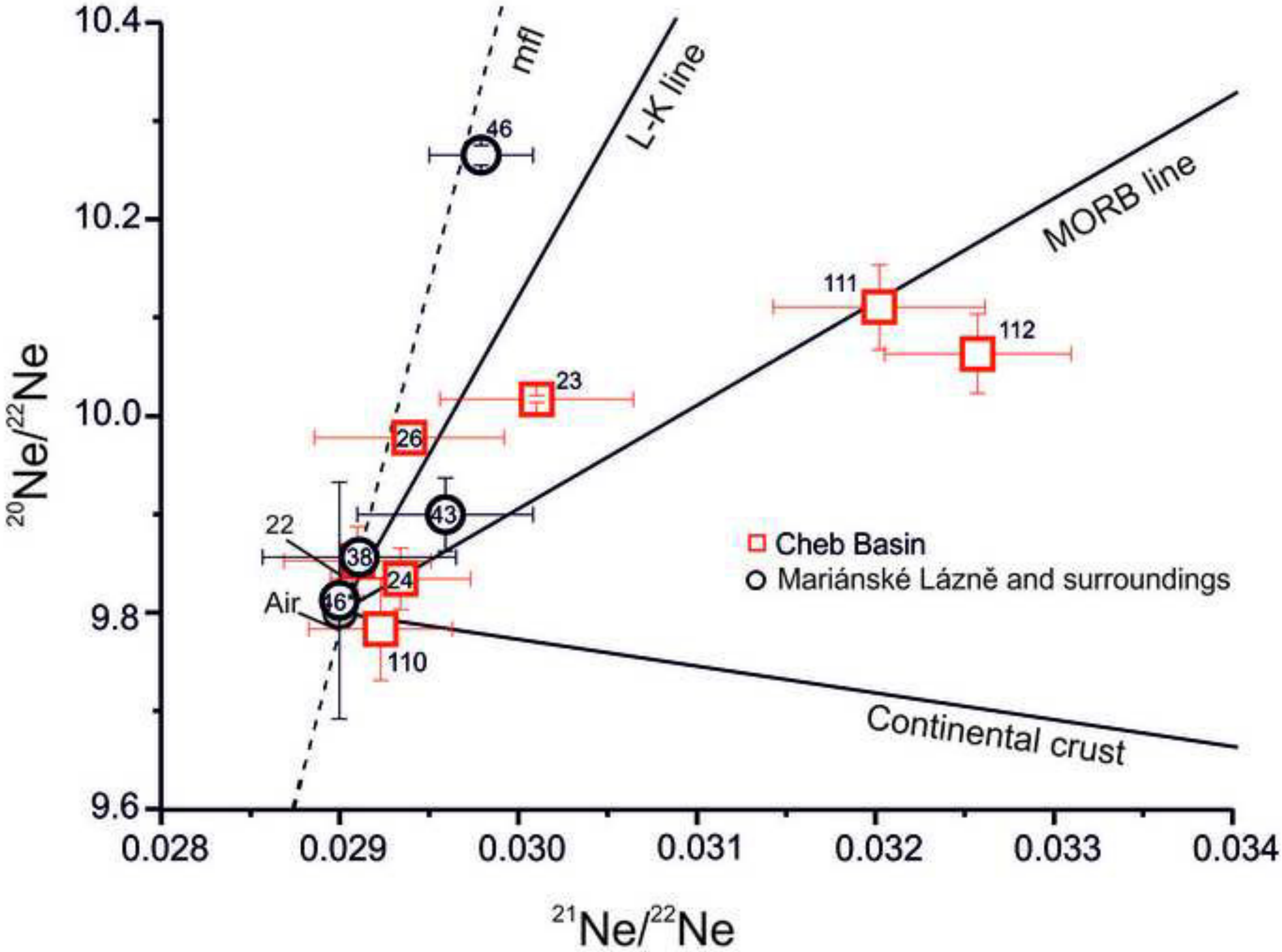

Figure
Click here to download high resolution image

Figure

Click here to download high resolution image

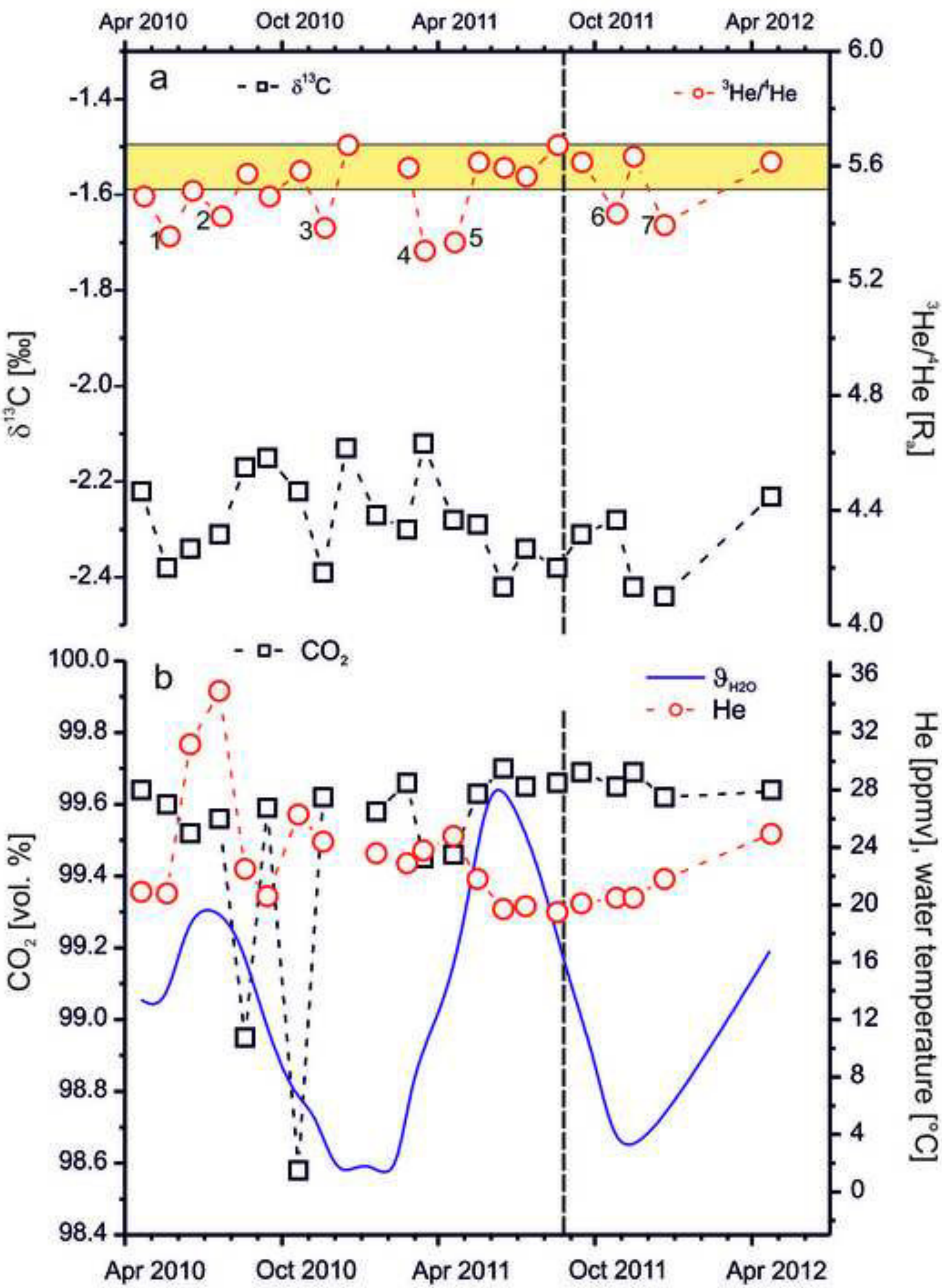

Figure
Click here to download high resolution image

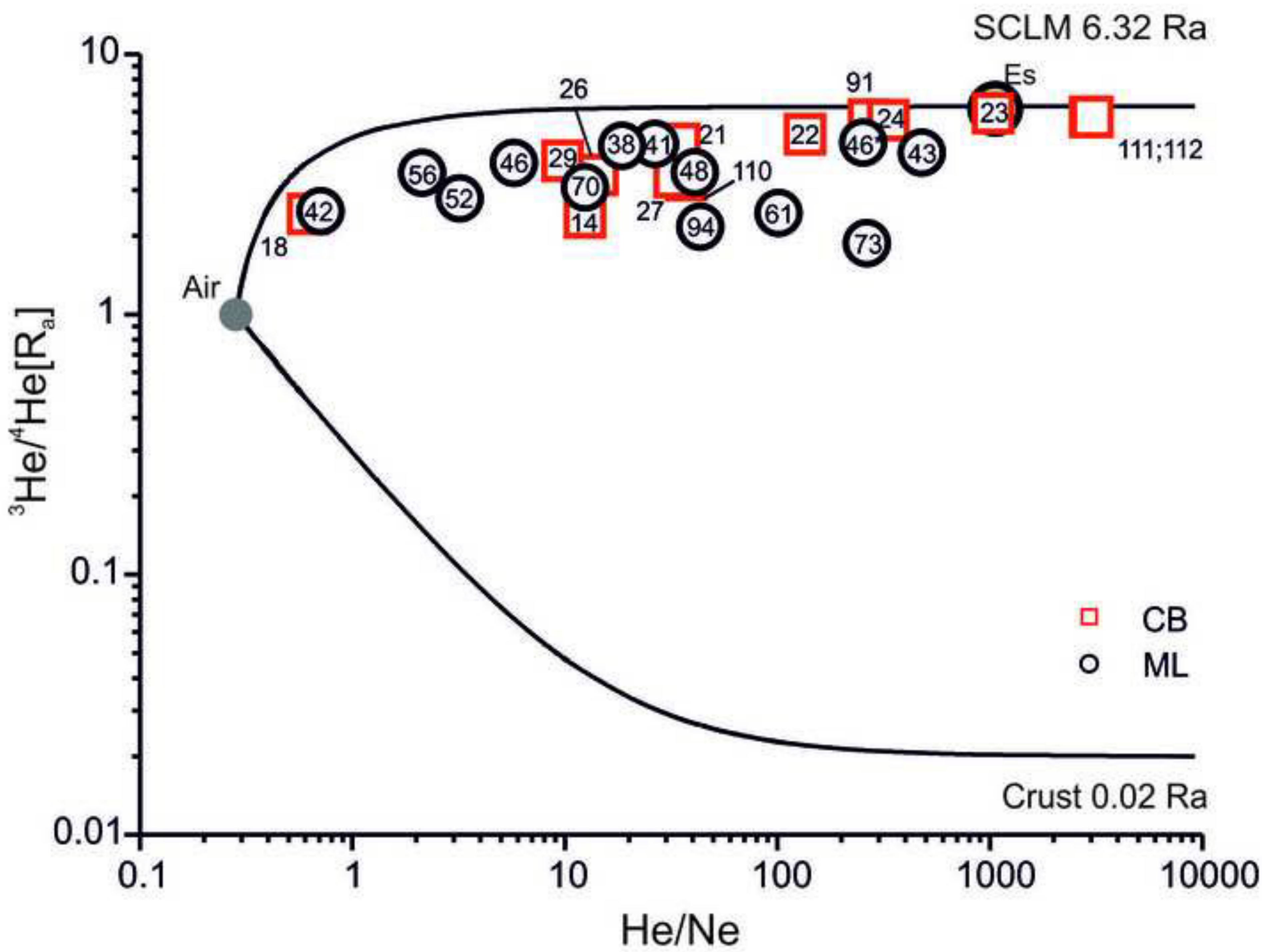

Figure
Click here to download high resolution image

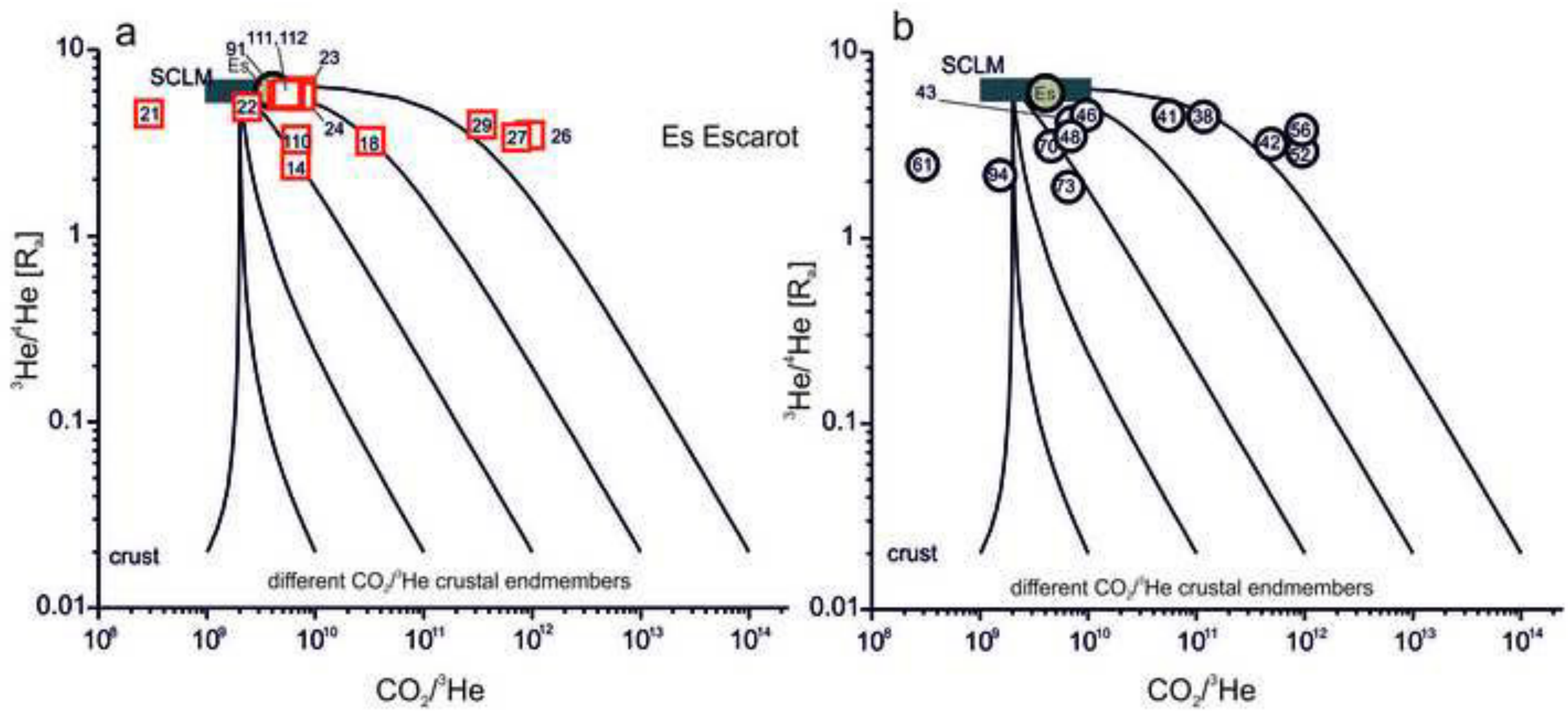

Figure
Click here to download high resolution image

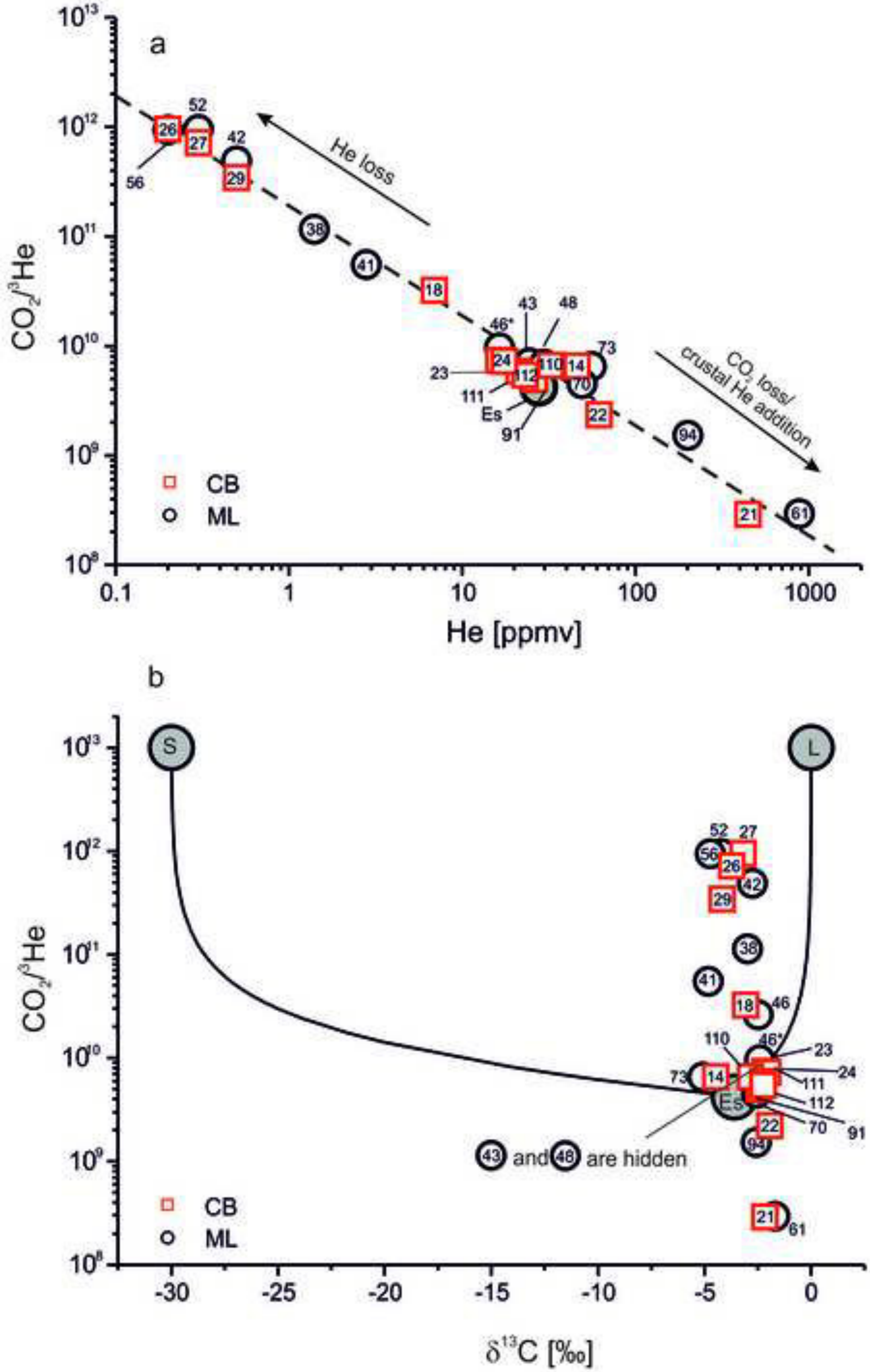

Figure

Click here to download high resolution image

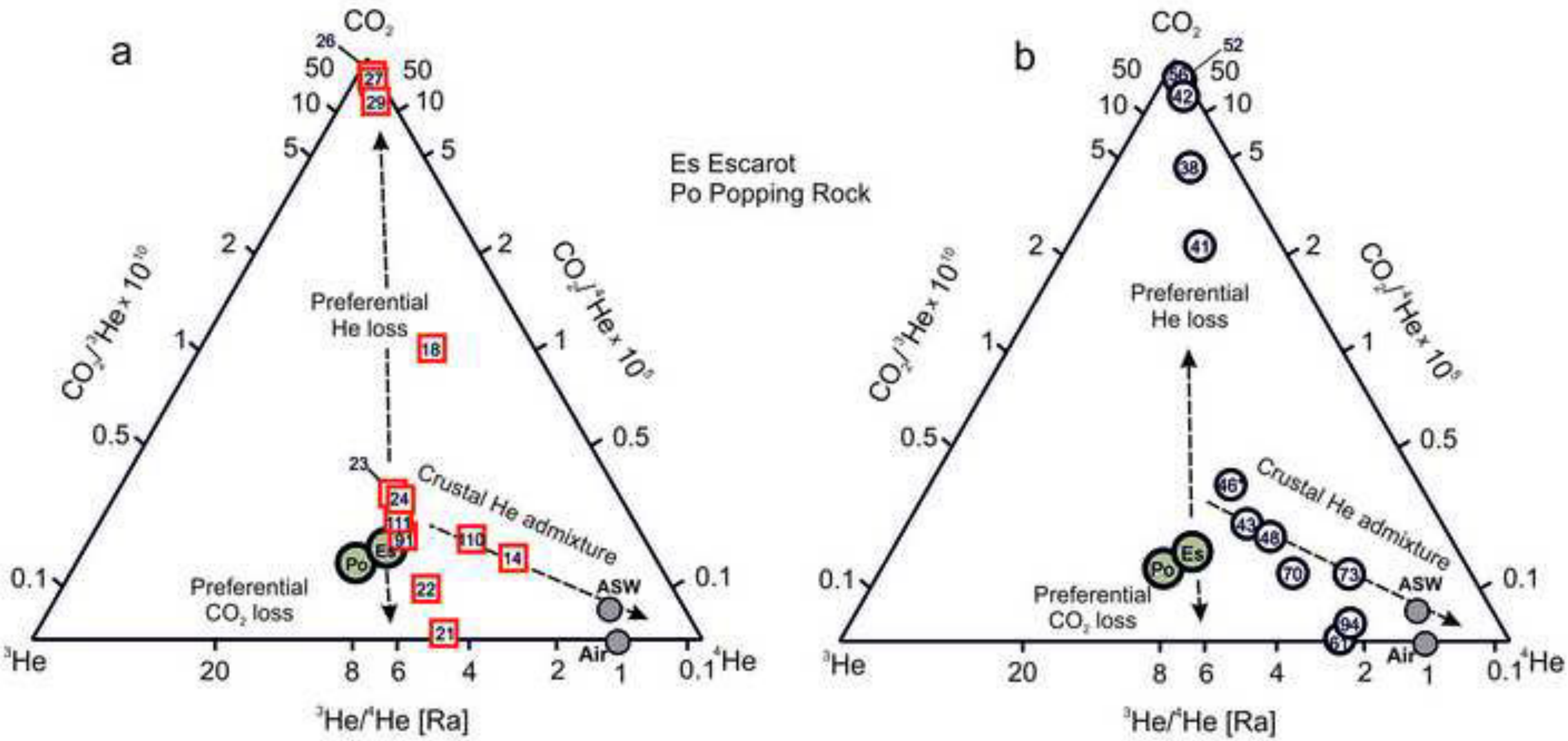

Figure
Click here to download high resolution image

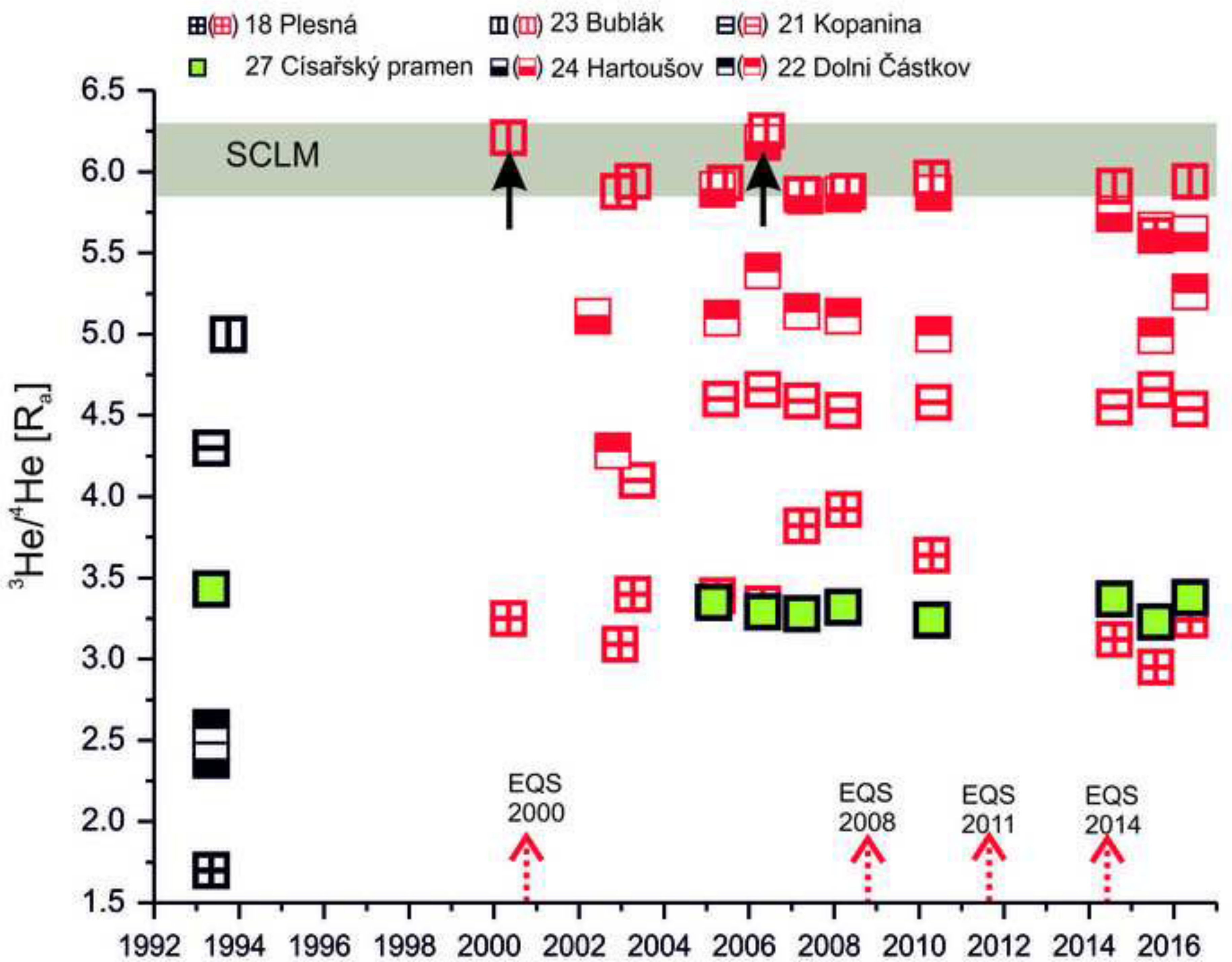

Table

Click here to download Table: Table 1.docx

Table 1 Classification, field data and gas and isotopic composition of the free gas phase of degassing locations in the Vogtland and NW Bohemia region

No.	Location	Date	GPS Coordinates (WGS 84) °N	°E	Type of degassing	ϑ_{H2O} °C	Cond. µS/cm	pH	CO_2 vol.%	He ppmv	H_2 ppmv	O_2 vol.%	N_2 vol.%	Ar vol.%	CH_4 ppmv	$\delta^{13}C$ ‰	He/Ne	$(^3He/^4He)_c$ R_a
Degassing center Cheb Basin (CB) and surroundings																		
22	Dolní Častkov	17.05.2011	50.167	12.497	mofette	11.1	490	3.53	99.37	39.9	b.d.l.	0.074	0.54	0.009	43.7	-2.03	228	5.14
22	Dolní Častkov	16.06.2011	50.167	12.497	mofette	15.5	401	4.49	99.50	38.6	b.d.l.	0.045	0.44	0.007	26.7	-2.09	177	4.91[a]
22	Dolní Častkov	12.07.2011	50.167	12.497	mofette	17.0	370	5.03	99.46	35.7	b.d.l.	0.060	0.47	0.009	19.4	-2.10	105	5.03[a]
22	Dolní Častkov	18.08.2011	50.167	12.497	mofette	16.3	415	5.23	99.44	35.4	b.d.l.	0.067	0.48	0.009	22.5	-2.05	n.d.	n.d.
22	Dolní Častkov	15.09.2011	50.167	12.497	mofette	14.8	254	4.97	99.49	35.3	b.d.l.	0.090	0.41	0.008	23.2	-2.04	511	5.12
22	Dolní Častkov	26.10.2011	50.167	12.497	mofette	10.2	n.d.	n.d.	99.53	36.8	b.d.l.	0.038	0.42	0.007	16.3	-1.99	456	5.01[a]
22	Dolní Častkov	15.11.2011	50.167	12.497	mofette	7.5	337	4.39	99.47	37.1	b.d.l.	0.055	0.46	0.007	16.1	-1.99	469	5.05[a]
22	Dolní Častkov	21.12.2011	50.167	12.497	mofette	5.0	233	4.40	99.42	38.9	b.d.l.	0.063	0.50	0.008	17.8	-1.92	172	4.99[a]
22	Dolní Častkov	24.04.2012	50.167	12.497	mofette	7.1	299	4.17	99.43	48.1	b.d.l.	0.060	0.50	0.008	15.4	-2.06	277	5.05[a]
23	Bublák	17.05.2011	50.143	12.454	mofette	11.2	132	4.49	99,50	17.5	b.d.l.	0.131	0.35	0.008	41.5	-2.10	163	5.94
23	Bublák	16.06.2011	50.143	12.454	mofette	13.0	133	4.56	99.60	18.0	b.d.l.	0.104	0.29	0.007	49.0	-2.14	123	5.89
23	Bublák	12.07.2011	50.143	12.454	mofette	13.8	121	4.29	99.57	16.8	b.d.l.	0.110	0.31	0.008	19.9	-2.09	691	5.89
23	Bublák	18.08.2011	50.143	12.454	mofette	13.8	123	4.43	99.62	15.7	b.d.l.	0.098	0.28	0.007	3.7	-2.16	203	5.81[a]
23	Bublák	15.09.2011	50.143	12.454	mofette	12.2	130	4.46	99.65	14.6	b.d.l.	0.081	0.26	0.006	3.6	-2.19	597	5.94
23	Bublák	26.10.2011	50.143	12.454	mofette	8.9	130	4.38	99.59	17.6	b.d.l.	0.107	0.29	0.007	4.4	-2.11	269	5.93
23	Bublák	15.11.2011	50.143	12.454	mofette	5.7	144	4.56	99.61	16.2	b.d.l.	0.105	0.28	0.006	9.4	-2.20	554	5.82[a]
23	Bublák	21.12.2011	50.143	12.454	mofette	4.4	120	4.53	99.71	15.8	b.d.l.	0.070	0.21	0.004	4.3	-2.14	592	5.89
23	Bublák	24.04.2012	50.143	12.454	mofette	8.8	121	4.53	99.59	21.3	b.d.l.	0.104	0.29	0.006	6.2	-2.23	232	5.60[a]
24	Hartoušov	24.04.2012	50.132	12.464	mofette	10.4	158	5.01	99.31	24.6	b.d.l.	0.217	0.46	0.011	7.5	-2.02	305	5.65[a]
14a	BB, Wettinquelle	07.08.2014	50.221	12.304	spring	12.0	1760	5.90	99.82	1.6	b.d.l.	0.011	0.16	0.004	23.0	-4.71	87	2.33
18	Plesná	06.08.2014	50.226	12.370	spring	9.6	215	5.30	98.77	33.6	b.d.l.	0.302	0.91	0.019	4.1	-3.19	0.55	3.12
21	Kopanina	05.08.2014	50.206	12.458	spring	9.4	231	4.62	79.64	461.0	b.d.l.	0.691	19.30	0.305	109	-2.18	207	4.56
23	Bublák	05.08.2014	50.143	12.454	mofette	14.3	145	n.d.	99.60	16.8	b.d.l.	0.103	0.29	0.007	4.3	-2.21	438	5.92
24	Hartoušov	05.08.2014	50.132	12.464	mofette	17.6	172	4.88	99.30	22.4	b.d.l.	0.213	0.47	0.011	14.8	-2.03	157	5.74
27	Cisařský pramen	05.08.2014	50.148	12.403	spring	17.6	6120	6.01	99.79	0.6	b.d.l.	0.065	0.14	0.003	4.4	-3.81	52	3.37
26	Soos mofette	05.08.2014	50.149	12.412	mofette	16.6	3790	5.84	99.95	0.05	0.2	0.013	0.04	0.001	0.5	-3.27	24	3.55
29	Kyselecký Hamr	06.08.2014	50.015	12.465	spring	9.0	2610	5.91	99.74	0.5	b.d.l.	0.074	0.18	0.005	20.1	-4.30	24	3.94
91	Skalná, Nová Ves II	05.08.2014	50.177	12.410	mofette	20.1	294	5.11	99.53	26.0	b.d.l.	0.096	0.36	0.008	5.9	-2.44	305	5.61
14	BB, Eisenquelle	29.07.2015	50.222	12.299	spring	9.6	1380	5.40	99.50	45.8	0.5	0.028	0.46	0.010	2.8	-4.48	14	2.39
14a	BB, Wettinquelle	29.07.2015	50.221	12.304	spring	11.7	1806	5.82	99.89	0.7	0.6	0.010	0.10	0.003	13.3	-4.81	54	2.36[a]
18	Plesná	29.07.2015	50.226	12.370	spring	9.7	235	5.08	99.34	15.2	b.d.l	0.160	0.48	0.012	3.7	-3.11	0.44	2.96

21	Kopanina	28.07.2015	50.206	12.458	spring	9.6	232	4.35	81.15	463.5	b.d.l.	0.456	18.08	0.254	124	-2.75	36	4.67
22	Dolní Častkov	28.07.2015	50.167	12.497	mofette	n.d.	n.d.	n.d.	99.35	48.2	b.d.l.	0.065	0.57	0.009	18.7	-1.88	46	4.99[a]
23	Bublák	28.07.2015	50.143	12.454	mofette	14.4	107	4.25	99.32	22.5	b.d.l.	0.195	0.47	0.012	5.5	-2.12	34	5.62[a]
24	Hartoušov	28.07.2015	50.143	12.454	mofette	15.4	193	4.77	99.37	18.9	b.d.l.	0.172	0.44	0.010	8.5	-2.08	52	5.64[a]
26	Soos mofette	28.07.2015	50.149	12.412	mofette	16.2	5350	5.90	99.75	3.8	36.5	0.004	0.24	0.005	3.2	-3.03	11.5	3.45
27	Cisařský pramen	28.07.2015	50.148	12.403	spring	17.6	6380	6.02	99.85	0.3	1.9	0.046	0.10	0.003	3.9	-3.68	22	3.22
29	Kyselecký Hamr	29.07.2015	50.015	12.465	spring	8.8	2600	5.78	99.67	12.0	0.3	0.024	0.30	0.006	5.7	-4.20	15	3.92
18	Plesná	18.05.2016	50.226	12.370	spring	8.4	245	5.50	99.33	6.9	b.d.l.	0.203	0.45	0.012	2.8	-3.08	0.69	3.24
21	Kopanina	17.05.2016	50.206	12.458	spring	8.5	229	4.64	81.39	445.2	b.d.l.	0.245	18.07	0.241	84.9	-2.17	39	4.54
22	Dolní Častkov	18.05.2016	50.167	12.497	mofette	n.d.	n.d.	n.d.	99.33	61.5	b.d.l.	0.018	0.63	0.009	19.5	-1.94	59	5.28
23	Bublák	17.05.2016	50.143	12.454	mofette	10.2	113	4.64	99.56	16.3	b.d.l.	0.115	0.32	0.008	2.8	-2.17	1113	5.95
24	Hartoušov	17.05.2016	50.132	12.464	mofette	10.9	168	4.96	98.63	17.5	b.d.l.	0.325	1.02	0.018	8.1	-2.03	357	5.60
26	Soos mofette	18.05.2016	50.149	12.412	mofette	12.6	6140	6.33	99.79	0.2	0.2	0.057	0.15	0.004	0.7	-3.20	15	3.50
27	Cisařský pramen	18.05.2016	50.148	12.403	spring	17.4	6280	5.84	99.71	0.3	0.3	0.093	0.19	0.005	4.0	-3.72	37	3.38
29	Kyselecký Hamr	18.05.2016	50.015	12.465	spring	8.8	2580	5.93	99.52	0.5	b.d.l.	0.138	0.33	0.009	3.4	-4.18	11	3.97
110	FL Mariin pramen	03.09.2009	50.015	12.465	mofette	n.d.	n.d.	n.d.	98.87	30.2	b.d.l.	0.019	1.05	0.033	55.9	-2.84	261	3.24
110	FL Mariin pramen	24.11.2014	50.114	12.350	mofette	n.d.	n.d.	n.d.	98.85	32.4	b.d.l.	0.019	1.09	0.026	67.4	-2.85	215	3.36
111	Hartoušov (HJB-1)	18.07.2016	50.133	12.463	borehole	n.d.	n.d.	n.d.	99.89	21.3	b.d.l.	0.010	0.10	0.002	7.9	-2.28	3172	5.75
112	Hartoušov (1H-031)	18.07.2016	50.133	12.463	borehole	n.d.	n.d.	n.d.	99.87	23.1	b.d.l.	0.015	0.11	0.003	5.0	-2.25	3267	5.75
Degassing Center Mariánské Lázně (ML) and surroundings																		
38	Prameny	07.10.2014	50.047	12.727	spring	8.0	753	6.53	98.64	1.4	b.d.l.	0.430	0.91	0.020	10.6	-2.99	23	4.60
41	Louka, Grünska kys.	08.10.2014	50.067	12.788	spring	10.1	1915	6.10	97.68	2.8	b.d.l.	0.070	2.20	0.049	31.8	-4.82	30	4.56
42	Farska kyselká	07.10.2014	50.015	12.724	spring	8.1	558	5.73	99.55	0.5	b.d.l.	0.104	0.33	0.009	85.0	-2.76	0.77	3.22
43	Smrad'och	07.10.2014	50.013	12.717	mofette	9.6	663	2.87	99.40	24.4	b.d.l.	0.113	0.47	0.010	80.1	-2.23	501	4.17
*46	ML Mariiny	10.05.2005	49.976	12.709	mofette	n.d.	n.d.	n.d.	99.77	16.4	b.d.l.	0.033	0.18	0.003	25.1	-2.42	357	4.57
46	ML Mariiny	25.11.2014	49.976	12.709	mofette	n.d.	n.d.	n.d.	93.64	6.4	b.d.l.	1.337	4.97	0.046	61.8	-2.49	6.1	4.08
48	Sirňák, Podhorní Vrch	18.05.2016	49.978	12.788	mofette	15.0	615	2.87	99.30	29.7	b.d.l.	0.101	0.55	0.009	366	-2.39	46	3.53
52	Čiperka	08.10.2014	49.912	12.785	spring	10.7	1811	6.13	99.79	0.3	b.d.l.	0.070	0.14	0.005	2.4	-4.22	3.6	2.93
56	Otročin	08.10.2014	50.017	12.894	spring	8.2	1592	6.00	99.87	0.2	b.d.l.	0.027	0.10	0.003	7.1	-4.74	2.3	3.81
61	Křepkovice	25.11.2014	49.931	12.878	spring	8.1	420	5.48	88.49	880.5	b.d.l.	1.170	9.80	0.241	2097	-1.71	114	2.46
70	Kokašice	26.11.2014	49.878	12.955	spring	6.1	430	5.20	96.03	49.1	b.d.l.	0.223	3.55	0.075	1237	-2.57	14	3.12
73	Břetisl., Na Hadovce	08.10.2014	49.863	12.972	spring	8.3	875	5.80	94.74	55.6	b.d.l.	0.485	4.19	0.104	4785	-5.08	297	1.89
Degassing Center Karlovy Vary (KV)																		
94	Dorotka	26.11.2014	50.218	12.889	spring	21.0	1551	5.15	92.86	201.0	b.d.l.	0.025	6.98	0.114	13.6	-3.58	49	2.17

n.d. not determined, b.d.l. below detection limit, *46 before reconstruction, BB= Bad Brambach, FL=Františkovy Lázně, superscript "a" marks seismically influenced ^{3}He/^{4}He ratios

Table

Click here to download Table: Table 2.docx

No	Location	Date	$^4He/^{20}Ne$	$(^3He/^4He)_c$ R_a	$^{20}Ne/^{22}Ne$	$^{21}Ne/^{22}Ne$	$\delta^{20}Ne$	$\delta^{21}Ne$	$^{40}Ar/^{36}Ar$	$^{38}Ar/^{36}Ar$
22	Dolní Častkov	18.05.2016	63	5.28±0.12	9.850±0.035	0.02910±0.00041	0.51	0.34	318.2±3.0	0.1880±0.0015
23	Bublák	17.05.2016	1172	5.95±0.12	10.014±0.034	0.03011±0.00054	2.18	3.83	461.7±2.7	0.1874±0.0011
24	Hartoušov	17.05.2016	376	5.59±0.11	9.832±0.031	0.02934±0.00039	0.33	1.17	373.7±2.1	0.1880±0.0010
26	Soos	18.05.2016	16	3.50±0.07	9.975±0.017	0.02939±0.00053	1.79	1.34	297.0±1.4	0.1872±0.0010
110	FL Mariin pramen	24.11.2014	226	3.35±0.04	9.781±0.052	0.02923±0.00040	-0.19	0.79	315.6±1.6	0.1885±0.0010
111	Hartoušov (HJB-1)	18.07.2016	3340	5.75±0.12	10.107±0.043	0.03201±0.00059	3.13	10.38	1342±13	0.1883±0.0010
112	Hartoušov (1H-031b)	18.07.2016	3440	5.75±0.07	10.060±0.040	0.03256±0.00052	2.65	12.28	1430±9	0.1873±0.0010
38	Prameny	07.10.2014	24	4.59±0.09	9.854±0.016	0.02911±0.00054	0.55	0.38	301.9±1.5	0.1884±0.0011
43	Smrad'och	07.10.2014	527	4.17±0.09	9.897±0.037	0.02959±0.00049	0.99	2.03	377.6±3.2	0.1878±0.0012
*46	ML Mariiny	14.05.2003	140	4.48±0.09	9.81±0.12	0.0290±0.0013	0.10	0.0	562.4±5.9	0.1871±0.0010
46	ML Mariiny	25.11.2014	6.5	4.07±0.10	10.261±0.010	0.02979±0.00029	4.70	2.72	291.4±1.4	0.1844±0.0010

*46 before reconstruction, FL= Františkovy Lázně, ML= Mariánské Lázně

Table

Click here to download Table: Table 3.docx

Table 3 Monitoring of gas and isotopic composition of the free gas phase from the open clay pit Nová Ves II (no. 91) near the locality Skalná

Location	Date	ϑ_{H2O} °C	Cond. µS/cm	pH	CO_2 vol.%	He vpm	H_2 vpm	N_2 vol.%	O_2 vol.%	Ar vol.%	CH_4 vpm	$\delta^{13}C$ ‰	$\delta^{15}N$ ‰	He/Ne	$(^3He/^4He)_c$ R_a
Skalná	12.03.2001	11.3	250	5.50	99.48	18.2	b.d.l.	0.43	0.07	0.010	4.7	-2.22	n.d.	220	5.41[a]
Skalná	13.05.2003	n.d.	n.d.	n.d.	99.25	12.6	b.d.l.	0.51	0.23	0.013	3.5	-2.21	-0.1	35	5.60
Skalná	27.04.2006	n.d.	n.d.	n.d.	99.49	10.4	b.d.l.	0.38	0.11	0.009	3.7	-2.30	n.d.	140	5.91[b]
Skalná	25.04.2007	n.d.	n.d.	n.d.	98.92	10.9	12.2	0.74	0.32	0.017	3.4	-1.53	-0.5	51	5.71
Skalná	25.06.2008	n.d.	n.d.	n.d.	99.55	31.0	4.6	0.38	0.06	0.009	6.8	-2.38	-0.9	521	5.64
Skalná	29.10.2009	11.0	192	4.95	99.74	19.8	2.6	0.21	0.03	0.004	3.3	-2.38	-1.4	360	5.37[a]
Skalná	20.04.2010	14.0	277	5.11	99.64	20.9	1.5	0.27	0.07	0.007	4.9	-2.22	0.6	1000	5.50
Skalná	20.05.2010	13.1	93	5.50	99.60	20.8	b.d.l.	0.31	0.08	0.006	4.4	-2.38	-0.4	1050	5.36[a]
Skalná	16.06.2010	20.5	201	5.04	99.52	31.2	b.d.l.	0.37	0.10	0.008	6.0	-2.34	0.6	3900	5.52
Skalná	20.07.2010	20.9	123	n.d.	99.56	34.9	1.1	0.35	0.08	0.007	7.8	-2.31	0.3	308	5.43[a]
Skalná	19.08.2010	18.5	110	4.99	98.95	22.5	b.d.l.	0.81	0.23	0.015	6.5	-2.17	-0.9	1060	5.58
Skalná	14.09.2010	13.0	336	5.28	99.59	20.6	0.8	0.32	0.09	0.007	6.2	-2.15	-0.6	31	5.50
Skalná	20.10.2010	7.0	358	5.34	98.58	26.3	1.4	1.06	0.33	0.020	6.3	-2.22	-1.3	408	5.59
Skalná	18.11.2010	6.0	338	4.90	99.62	24.4	0.4	0.29	0.08	0.006	2.6	-2.39	-1.8	3750	5.39[a]
Skalná	15.12.2010	0.5	303	5.09	n.d.	n.d.	n.d.	n.d.	n.d.	n.d.	n.d.	-2.13	-1.3	3506	5.68
Skalná	19.01.2011	2.6	411	5.47	99.58	23.6	0.4	0.33	0.08	0.007	10.8	-2.27	-0.5	n.d.	n.d.
Skalná	24.02.2011	0.0	452	5.18	99.66	22.9	b.d.l.	0.27	0.06	0.006	7.3	-2.30	-1.3	245	5.60
Skalná	15.03.2011	8.6	388	5.50	99.45	23.8	b.d.l.	0.40	0.14	0.008	7.5	-2.12	0.4	1080	5.31[a]
Skalná	19.04.2011	13.0	386	5.52	99.46	24.8	b.d.l.	0.40	0.13	0.008	5.6	-2.28	1.2	804	5.34[a]
Skalná	17.05.2011	18.8	255	4.96	99.63	21.8	b.d.l.	0.30	0.06	0.006	11.4	-2.29	0.8	165	5.62
Skalná	16.06.2011	30.2	373	5.34	99.70	19.7	0.9	0.24	0.05	0.005	8.0	-2.42	-2.5	2491	5.60
Skalná	12.07.2011	29.3	426	5.50	99.65	19.9	b.d.l.	0.28	0.06	0.006	6.0	-2.34	0.6	113	5.57
Skalná	18.08.2011	23.8	396	5.10	99.66	19.5	b.d.l.	0.28	0.05	0.005	5.6	-2.38	n.d.	5089	5.68
Skalná	15.09.2011	17.0	378	5.18	99.69	20.1	b.d.l.	0.26	0.05	0.005	6.2	-2.31	n.d.	469	5.62
Skalná	26.10.2011	n.d.	n.d.	n.d.	99.65	20.5	b.d.l.	0.28	0.06	0.006	6.6	-2.28	-0.6	2306	5.44[a]
Skalná	15.11.2011	3.6	310	5.10	99.69	20.5	b.d.l.	0.25	0.05	0.005	5.8	-2.42	n.d.	611	5.64
Skalná	21.12.2011	2.3	239	5.10	99.62	21.8	b.d.l.	0.30	0.07	0.006	8.1	-2.44	-0.1	348	5.40[a]
Skalná	25.04.2012	17.6	214	4.97	99.64	24.9	b.d.l.	0.29	0.07	0.006	6.9	-2.23	-1.5	991	5.62
Skalná	05.08.2014	20.1	294	5.11	99.53	26.0	b.d.l.	0.36	0.10	0.008	5.9	-2.44	-0.5	305	5.61

n.d. not determined, b.d.l below detection limit, superscript a marks seismically influenced $^3He/^4He$ ratios, superscript b indicates a hidden magmatic process

Table
Click here to download Table: Table 4.docx

Table 4 Comparison of isotope ratios at selected degassing sites between 1993 and 2016

No.	Location	Date	$\delta^{13}C$ ‰	$(^3He/^4He)_c$ R_a	SCLM-He %
Degassing center Cheb Basin (CB) and surroundings					
18	Plesná	04.05.1993	-3.0	1.70	27
		18.05.2016	-3.1	3.24	51
21	Kopanina	05.05.1993	-2.4	4.30	68
		17.05.2016	-2.2	4.54	72
22	Dolní Častkov	04.05.1993	-1.9	2.58	41
		18.05.2016	-1.9	5.28	84
23	Bublák	29.09.2003	-2.1	5.01	79
		17.05.2016	-2.2	5.95	94
24	Hartoušov	05.05.1993	-2.1	2.38	38
		17.05.2016	-2.0	5.60	89
27	Cisařský pramen	05.05.1993	-3.6	3.43	54
		18.05.2016	-3.7	3.38	54
29	Kyselecký Hamr	07.05.1993	-4.2	3.45	55
		18.05.2016	-4.2	3.97	63
Degassing Center Mariánské Lázně (ML) and surroundings					
38	Prameny	08.05.1993	-3.1	4.87	77
		07.10.2014	-3.0	4.60	73
41	Louka, Grünska kys.	08.05.1993	-5.4	4.46	71
		08.10.2014	-4.8	4.56	72
42	Farska kyselká	30.05.1993	-2.8	3.94	62
		07.10.2014	-2.8	3.22	51
46	ML Mariiny	20.04.1994	-2.7	4.73	75
		10.05.2005	-2.4	4.57	72
48	Sirňák, Podhorní Vrch	30.09.1993	-2.4	3.34	53
		18.05.2016	-2.4	3.53	56
52	Čiperka	06.06.1992	-4.1	3.32	53
		08.10.2014	-4.2	2.93	46
56	Otročin	08.05.1993	-4.6	4.09	65
		08.10.2014	-4.7	3.81	60
61	Křepkovice	27.04.1994	-2.9	2.34	37
		25.11.2014	-1.7	2.46	39
70	Kokašice	01.10.1993	-3.1	2.91	46
		26.11.2014	-2.6	3.12	49
73	Břetisl., Na Hadovce	11.05.1993	-5.5	1.90	30
		08.10.2014	-5.1	1.89	30
Degassing Center Karlovy Vary (KV)					
94	Dorotka	08.01.2001	-3.0	2.35	37
		26.11.2014	-3.6	2.17	34

The data of locations from the CB and ML degassing centers (till 2008) were published in Bräuer et al. (2009)